Università degli Studi di Padova
Dipartimento di Biologia
Corso di Laurea Magistrale in Biotecnologie Industriali

Engineered nanogels with catalytic activity towards C-C bond formation

Relatore: Prof. Alessandro Moretto
Dipartimento di Scienze Chimiche

Controrelatore: Prof.ssa Silvia Gross
Dipartimento di Scienze Chimiche

Laureando: Beatrice Civili

Anno Accademico 2021/2022

SUMMARY

Abbreviations ..... **III**

Abstract ..... **IV**

1. Introduction **1**

1.1 Gold nanoparticles. 1

1.1.1 Gold nanoparticles optical properties 3

1.2 Protein corona 4

1.3 Bovine Serum Albumine (BSA) 6

1.4 Hydrogels 7

1.4.1 Free radical polymerization 10

1.5 Gold Nanoparticles - hydrogels hybrids 11

1.5.1 Poly (4-vinylpyridine) 13

1.5.2 Poly (N-Isopropylacrilamide) 13

1.6 Aldol Reactions 14

1.6.1 Aldol reaction Proline catalyzed 15

2 Materials and Methods **17**

2.1 Reagents and solvents 17

2.2 Equipements 18

2.2.1 UV- spectroscopy 18

2.2.2 High-Performance Liquid Chromatography. 18

2.2.3 Circular Dichroism 18

2.2.4 Nuclear Magnetic Resonance. 18

2.2.5 Transmission electron microscopy 18

2.2.6 Dynamic Light Scattering 19

2.3 Gold nanoparticles synthesis. 19

2.3.1 50 nm GNPs synthesis. 20

2.4 Nanoparticles stability with BSA. 20

2.5 BSA functionalization with L-Proline. 21

2.5.1 BSA functionalization with Boc-Proline-OH. 21

2.5.2 BSA functionalization with Proline NCA. 21

2.6 BSA-Pro protein corona formation around GNPs. 22

2.7 2.3.2 GNPs-(BSA-Pro) functionalization with Fluorescein isothiocyanate. 22
2.8 BSA functionalization with butanoic acid. 23
2.9 Polymerization 23
2.10 Etching 24
2.11 Solid-phase synthesis. 25
3 Results and Discussion 28
3.1 Nanoparticles synthesis 28
3.2 BSA protein corona on GNPs surface 32
3.3 GNPs stability 34
3.4 BSA modification with L-Proline. 35
3.5 BSA modification with Proline NCA 41
3.6 BSA-Pro protein corona formation. 44
3.7 Circular Dichroism analysis on BSA modified with Proline. 48
3.8 BSA labelling with FITC 50
3.9 Polymerization process. 53
3.9.1 BSA functionalization with Butanoic acid. 53
3.9.2 Polymerization p-NIPAM 54
3.10 Etching 57
3.11 Catalysis reaction 60
4 Conclusions 66
5 Future perspectives 67
6 Bibliography 69
Acknowledgments 75

ABBREVIATIONS

ABBREVIATIONS	RELATIVE CORRESPONDANCE
AA	Amino acid
ACN	Acetonitrile
AcOEt	Ethyl acetate
Boc	Tert-Butyloxycarbonyl
BA	bisacrilamide
CD	Circular dichroism
DCM	Dicloromethane
EDC	1-ethyl-3-(-3-dimethylaminopropyl) carbodiimide hydrochloride
Fmoc	Fluorenylmethyloxycarbonyl
GNPs	Gold nanoparticles
HPLC	High pressure liquid chromatography
HOAt	1-Hydroxy-7-azabenzotriazole
MeOH	Methanol
MW	Molecular weight
NaCt	Sodium citrate
NIPAM	N-isopropylacrilamide
PIP	Piperidine
TFA	Trifluoro acetic acid
TLC	Thin layer chromatography
tR	Retention time
UV	Ultra violet
V50	2,2′-azobis(2-methylpropionamidene) dihydrochloride

ABSTRACT

The aim of this experimental work is to combine three different nanomaterials to create a new one able to perform catalytic activity toward a C-C bond formation.

In our view, this work is an exploration of a novel chemical design and synthetic strategies at the nanometric-micrometric interface levels. Thus, starting from a natural and abundant protein, BSA, we chemically convert it into a catalytic platform acting toward an aldol condensation. This novel approach is then transferred to a metallic nanomaterial, composed by gold nanoparticle (GNPs). To do this we simply applied the Protein Corona effect, thus to strongly bind the novel catalyst over a GNPs. Interesting we still recovered catalytic activity. To move over, we built up a three-dimensional hydrogels network all around the functionalized GNPs. As a results, a core shell polymeric/metallic particle were obtained. Importantly, the modified protein stays at the core-shell interface level. While in one side the protein is only adsorbed on the GNPs, on the other side protein is covalently fixed to the polymeric matrix of the hydrogels trough the polymerization process. Finally, by sequestering the metallic core, the overall nanosystem now consists in an hollow hydrogel microsphere where the inner cavity is fully covered by the catalytic protein.

The resulting material performed enhanced catalytic properties, respect the counterparts in fully aqueous media.

1. INTRODUCTION

1.1 GOLD NANOPARTICLES.

Metal nanoparticles are studied and utilized in different fields, as drug delivery systems, catalysis, sensors, cancer therapy, for X-ray imaging or photodynamic therapy. Varying reaction parameters it's possible to obtain different structures, with different aspect (Fig.1) that affect their characteristics.[1] For this work we have decided to obtain spherical nanoparticles as much as possible.[2]

Figure 1 *Gold nanosystems with different shape and size.*

Inorganic nanoparticles, especially gold nanoparticles are very interesting and for this reason have been studied within the past 20 years. They are inorganic nanoparticles that consist of a gold atom inner core and stabilizing groups on the surface. They are very useful especially for their optical, electronic, physico-chemical features, while their low toxicity make them outstanding tools in biotechnology. Their typical surface plasmon resonance (SPR) band depends on their morphology and physiology. They are also very easy to synthetize. GNPs can be synthetized through different methods that can be divided in two classes, bottom up and top down. The method of Turkevich et al. with some slight modifications by Frens, remains yet the most preferred one for preparation of spherical gold nanoparticles in aqueous solution. As a matter of fact, Turkevich et al. were the first ones to demonstrate the possibility of changing the particles size, by controlling the concentration of the reducing agent and the temperature of the reaction.

Nanoparticles morphology is influenced by different reaction parameters, such as temperature, pH, reductants concentrations and time of reaction.

In this work we made use of the Turkevich method [3] that is performed in an aqueous medium by a reductant agent, sodium citrate that reduces $HAuCl^{4-}$ and stabilizes the solution of gold nanoparticles. The reaction is carried out at 120°C for about 20 minutes.

Indeed, the stabilization is essentially due to the mutual repulsion between neighbouring GNPs that is caused by the negative surface charge of the citrate layer. Citrate binding is relatively strong and its action as a chelator stabilizes surface reconstructions.

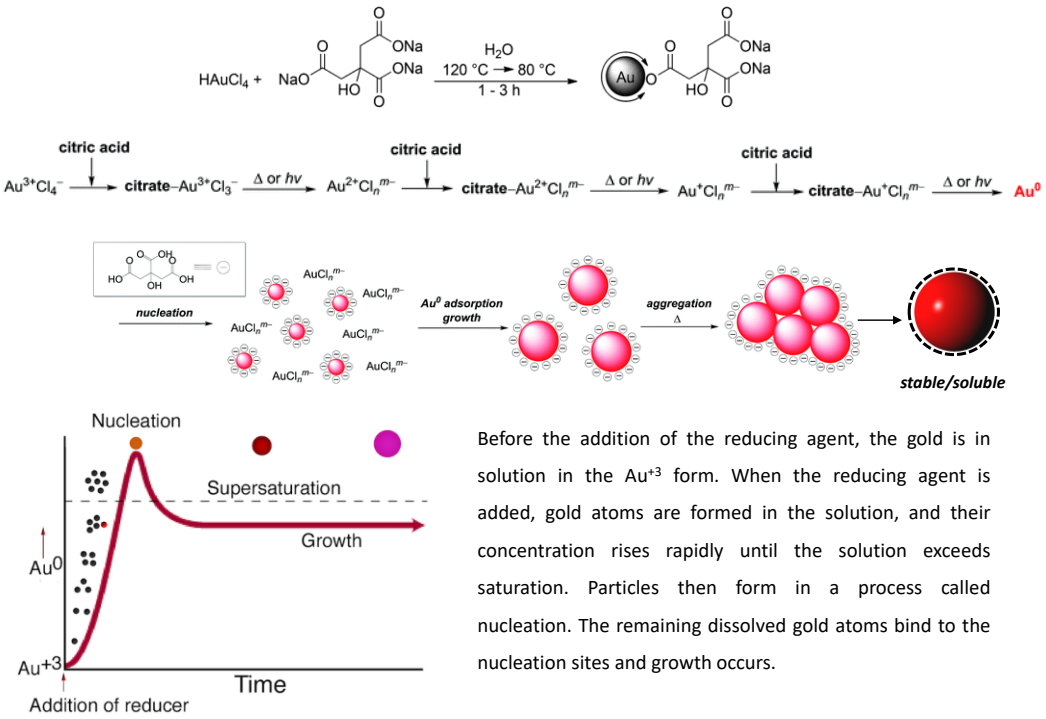

Before the addition of the reducing agent, the gold is in solution in the Au^{+3} form. When the reducing agent is added, gold atoms are formed in the solution, and their concentration rises rapidly until the solution exceeds saturation. Particles then form in a process called nucleation. The remaining dissolved gold atoms bind to the nucleation sites and growth occurs.

Figure 2 *Schematic representation of GNPs formation with Turkevich method. In the graph the curve describes LaMer model for GNPs nucleation and growth.*

The adsorption of the citrate consists of a strong coordination of the carboxyl oxygens to the surface that can involve one or more groups. Consequently, citrate limits the extension of the surface reconstruction. [4]

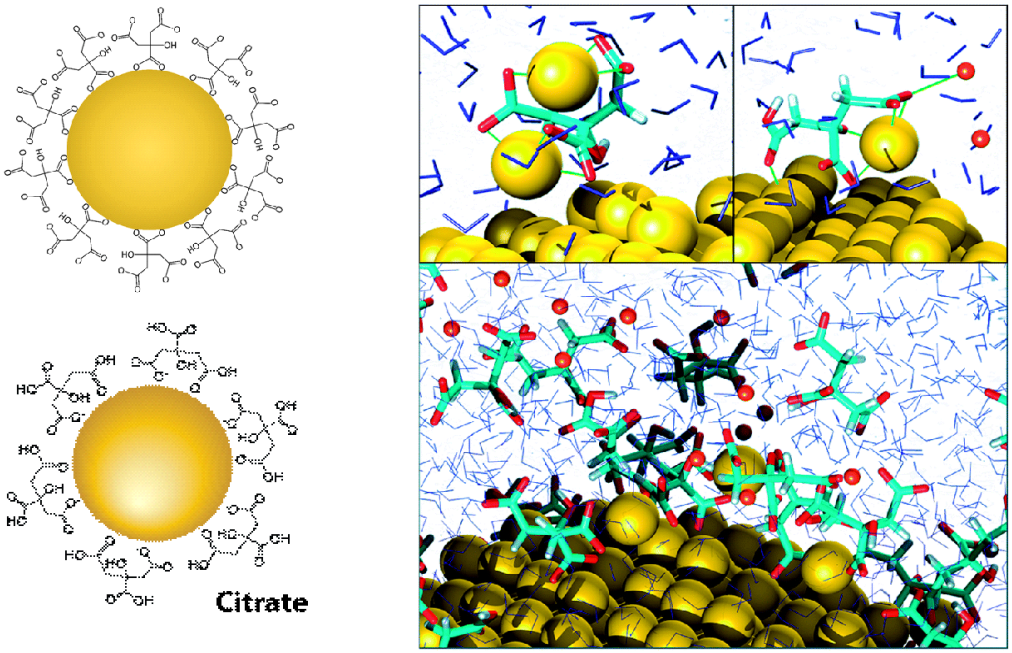

Figure 3 *Representation of adsorption and desorption of citrate on gold nanoparticles surface.*

Nanoparticles formation and their stability can be analysed in a first step through UV spectroscopy. In fact due to the nanoscale structure gold nanoparticles show a defined absorption peak at 520 nm thanks to surface plasmon resonance.

1.1.1 Gold nanoparticles optical properties

The GNPs optical properties are defined through their plasmon resonance, that is related to collective excitation of conduction electrons and concentrated in visible to infrared regions, depending on the structure, shape, and size of particle. High absorption coefficients of GNPs, permitting greater sensitivity in optical detection techniques than the common dyes. [5]

Light illumination of gold nanoparticles causes strong absorption or/and scattering at certain resonance wavelengths that depend to a large extent on their morphology and dielectric medium. Under light irradiation, the conduction electrons in a gold nanostructure are driven by an electric field for collective vibration at a resonant frequency relative to positive ions of the lattice. This phenomenon is known as localized surface plasmon resonance (LSPR).[5]

When light hits a gold nanoparticle, the free electrons of the metal form an electromagnetic field and begin collective oscillations relative to the lattice of positive ions at a frequency matching that of the incident light.

Surface Plasmon Resonance peak depends by different parameters, as nanoparticles aspect ratio, size, shape, or state of aggregation.

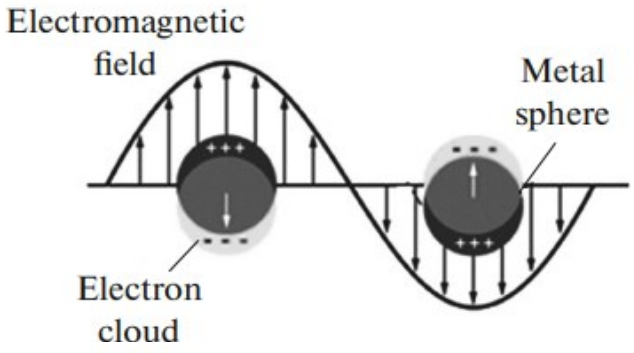

Figure 4 *Schematic illustration of collective vibration of the free electrons in a gold nanosphere, which are responsible for SPR.*

1.2 PROTEIN CORONA

GNP has been widely accepted to form protein corona rapidly when introduced into a biological medium. Proteins represent one of the major ligand used. Protein adsorption layer form a so called "corona", that not only can change nanoparticles characteristics but plays an interesting role in their interactions between themselves and other materials. The adsorption of proteins onto GNPs surface is known to depend on the surface property (chemical modifications) of GNPs, while in turn, the corona formation could change the physicochemical properties and further the biological patterns of GNP as well.[6]

Protein corona morphology depends on the type of protein, size, shape and charge of nanoparticles, reactions conditions, incubation time too. It acts as a "complex surfactant", it is what is ultimately seen by cells, so this determines the physiology response and interactions of NPs with living systems and so affects circulation

lifetime, cellular uptake, circulation lifetime, signalling, bio-diodistribution and toxicity.[6]

Protein corona formation is a kinetic process where initially there is a "soft protein corona" composed by loosely bound proteins in equilibrium with the free proteins in solution; then this condition evolves to an "hard protein corona" with tightly bound proteins that do not desorb. In J.Parac[7] work, they try to resume some analytical models to have quantitative data on protein corona formation, because is fundamental to understand how much this corona is stable, at which conditions, and at which concentrations. Proteins can adsorb and desorb to nanoparticles surface, and for this reason exists a model that describes this phenomenon, to understand equilibrium and kinetic properties of Protein-nanoparticle system.

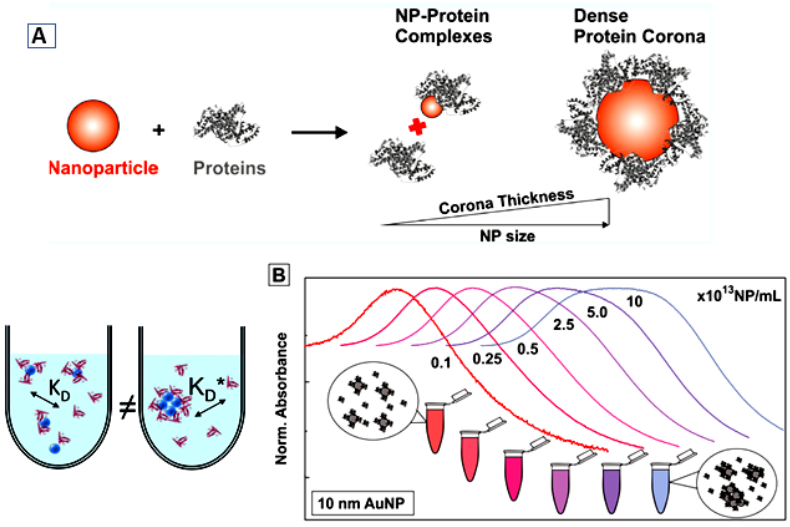

Figure 5 *Protein corona formation.* ***(A)*** *Corona thickness depends on how much protein can adsorb on NP.* ***(B)*** *Nanoparticles stability depends on protein concentration. Protein corona can avoid NPs precipitation.*

Protein corona is a smart solution to make nanoparticles invisible to immune system, when they are used in the case of drug delivery for example. There are huge studies that concern their adsorption on biomaterials surface, to avoid adverse reactions or material rejection.

1.3 BOVINE SERUM ALBUMINE (BSA)

Albumins are the most abundant (52-62%) total water-soluble proteins in blood plasma. They are bio macromolecules acting as transporter for carrying and delivering various endogenous and exogenous molecules, as ions or fatty acids.[8]

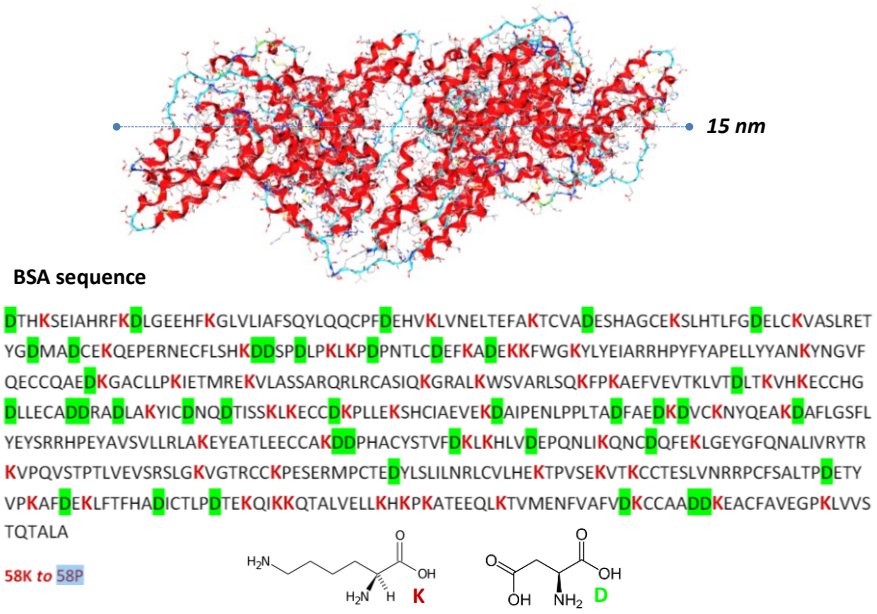

Figure 6 *BSA structure and amino acidic sequence. In green are underlined Aspartic residues, in red Lysine residues.*

Bovine serum albumin structure is similar to Human serum albumin (HAS), in fact is composed by a single polypeptide chain of 583 amino acids. This structure is stabilized by 17 disulfide bridges of cysteine (Cys) residues. It has a molecular weight of 66.8 kDa and it has three homologous domains I-III and each of them is constituted by two subdomains, A and B with unique binding properties.[8]

Thanks to X-ray diffraction six binding sites have been found in the hydrophobic cavities. For its peculiar structure and properties, especially for biocompatibility, they have took place in several fields. An example is drug-delivery and about this it is reported a study of BSA nanoparticles loaded with Doxorubicin for overcoming multidrug-resistant in cancer cells. Or in another case magnetic nanoparticles can be coated with BSA as curcumin carriers for anticancer drug. [2]

We have decided to use Bovine serum albumin (BSA or "Fraction V) to create a protein shell for GNPs. Because of its zwitterionic character at his isoelectric point, BSA can be used to label cationic silver (Ag+) or anionic gold (AuCl4-) ions. Moreover is water soluble, stable in a pH range of 4-9 and especially is stable in organic solvent, a thing that we have taken in consideration for this thesis purpose. From a chemical point of view the most interesting things are its disulphide bonds and sulfhydryl groups which allow protein to have interactions with organic and inorganic materials. [2]

In the case of BSA, there are different strategy to conjugate it with GNPs. As reported in literature[2] the most use for its simplicity and economy, is passive adsorption, which exploits covalent or non -covalent interactions. Other methods, are active adsorption, in situ strategy, desolvation cross-linking, emulsification or thermal gelation.

1.4 HYDROGELS

Nanogels and microgels are soft, deformable and penetrable objects with a gel-like structure that is swollen by the dispersing solvent. More generally gels are three-dimensional polymer networks that are swollen by a solvent such as water, as is for hydrogels. They represent a big research field for their properties that let them to be useful for a lot of applications.[9] These systems are considered "intelligent" because of their capability to sense environment, store and analyse information, and at the end respond to its surrounding. Moreover, to their physical characteristics introduced at the beginning, they are appreciated especially for the capability to respond to external stimuli, like pH, temperature, pressure, ionic strength and various analytes. Because of their good stability, easy preparation and composition heterogeneity, nanogels has been used in different fields of application, like drug delivery, catalysis, bio-sensing, cell therapy. There are some examples of micro- and nanogels that have been used to create biomimetic catalysts for biomass conversion reactions. Because of the capability of changing their physical state they can be applied as sensors. We report the example of glucose sensors. Very interesting is the case of phenylboronic-acid-functionalized microgels for their glucose-binding equilibrium-induced changes in microgel ionization, resulting in

tunable changes in microgel swelling, microgel net charge, and/or microgel transition temperature in response to glucose concentration changes.[10]

One of the main use, is for drug delivery, because of the porosity, composition, flexibility and colloidal stability.

For their structure and other properties, they have been applied as building block for bulk cell scaffolds. In other cases they can act as cell carriers too. An example of this are nonalginate microgels based on PNIPAM and on poly 2-oxazoline used as carriers for neuronal cells. [10]

The story of hydrogels throughout previous decades is shown in the figure below.

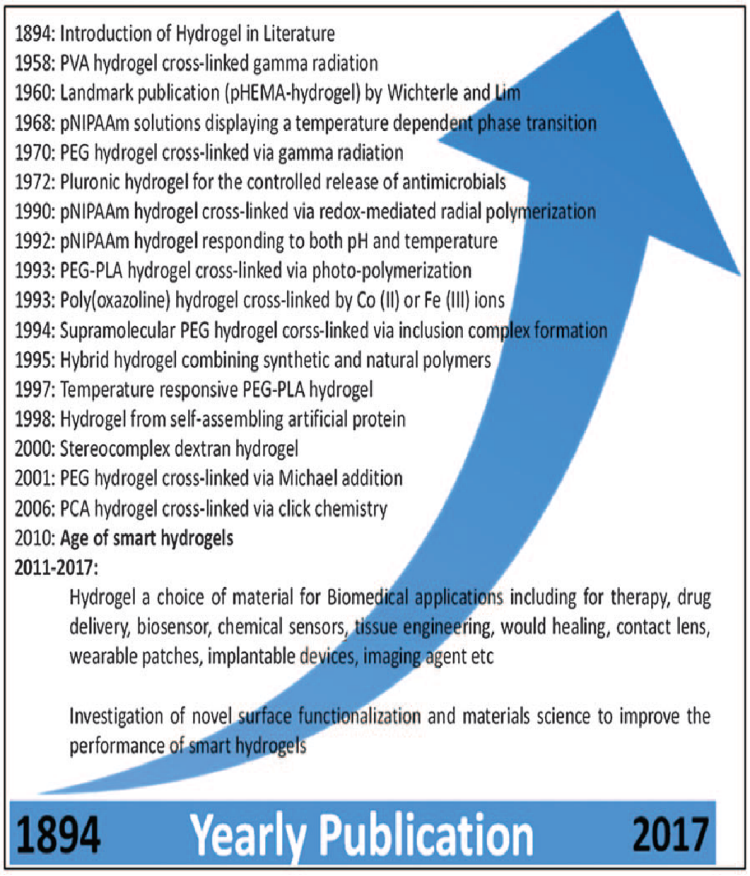

Figure 7 *Journey of hydrogels throughout previous decades.*

During time natural polymers with low mechanical strength are being replaced by synthetic polymers and this helps to avoid contamination like viruses or toxins, a typical risk of using animal-derived materials. From a technical point of view there are different synthesis method to obtain nanogels with controlled properties. In the work of Haag and his group[11] they highlight the progress in covalent and supramolecular crosslinking techniques to prepare micro- and nanogels.

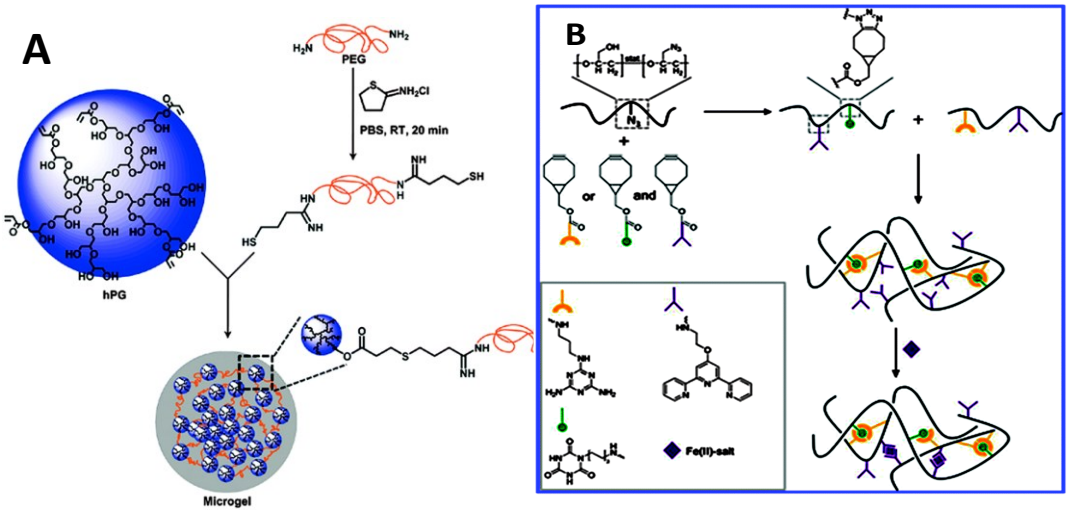

Figure 8 (A) *Formation of microgels by crosslinking hPG and PEG via Michael addition* ***(B)*** *Supramolecular hydrogel formation crosslinked by multiple hydrogen bonding and metal composition.*

Covalent crosslinking permits covalent coupling of the functional groups in the monomers or macromolecular precursors. Reactions include the free radical polymerization, click chemistries, Schiff-base reaction, thiol-disulphide exchange reaction and photoreaction. In figure 8(A) there is a representation of microgels formation through a click chemistry reaction, Michael addition. It consists in a base-catalysed nucleophilic addition of an enolate anion α,β-unsaturated carbonyl containing compound.[11]

With supramolecular crosslinking, nanogels formation is given by various physical interactions, as ionic, Hydrophobic and hydrogen bonding (Fig. 8B). The difference with the previous strategy is that this case does not need a crosslinking agent. In fact it could provide unwonted interactions with molecules. An important difference between the two methods is that nanogels prepared with supramolecular crosslinking may have less mechanical strength and stability, especially if we think in an in vivo condition.[11]

The most used is the free radical polymerization, for its flexibility, versatility, and simplicity. In fact, is usually conducted in an aqueous solution, in a temperature range between 60-80°C. Its flexibility is due to the fact that can be used with a large amount of different monomers and permits the introduction of different functional groups using comonomers or through post modifications. Polymerization begins with free radical, generated by initiator molecules, then monomers are crosslinked through crosslinkers to form nanogel network.[12] We have chosen poly (N-Isopropylacrilamide) to form nanogels, so the scaffold of the entire structure which is formed through free radical polymerization.

1.4.1 Free radical polymerization

The hydrogels formed in this work are obtained through a free radical polymerization (FRP). [13] In this synthesis we have used a vinyl termination to start polymerization.

Generally a polymerization has constituted by three steps:

1- Activation;
2- Propagation;
3- Termination.

During activation, there is the activation of initiator. Initiator is a molecule that can be activated with different stimuli, such as heat or light. Radical are then transferred from initiator to monomer molecules. The initiator can be activated through thermal decomposition, photolysis, redox reactions, electrochemical method or ionizing radiation. [14]

Then there is propagation. After the radical initiator is ready, it attacks a monomer. So, one time chain has been started, it propagates and other monomers add continuously. After a certain number of propagation states, there is a stop point, so termination, when a polymeric chain meets another polymeric chain growth during propagation phase. When these two radicals react, there is polymer formation with a specific number of repetitive units.

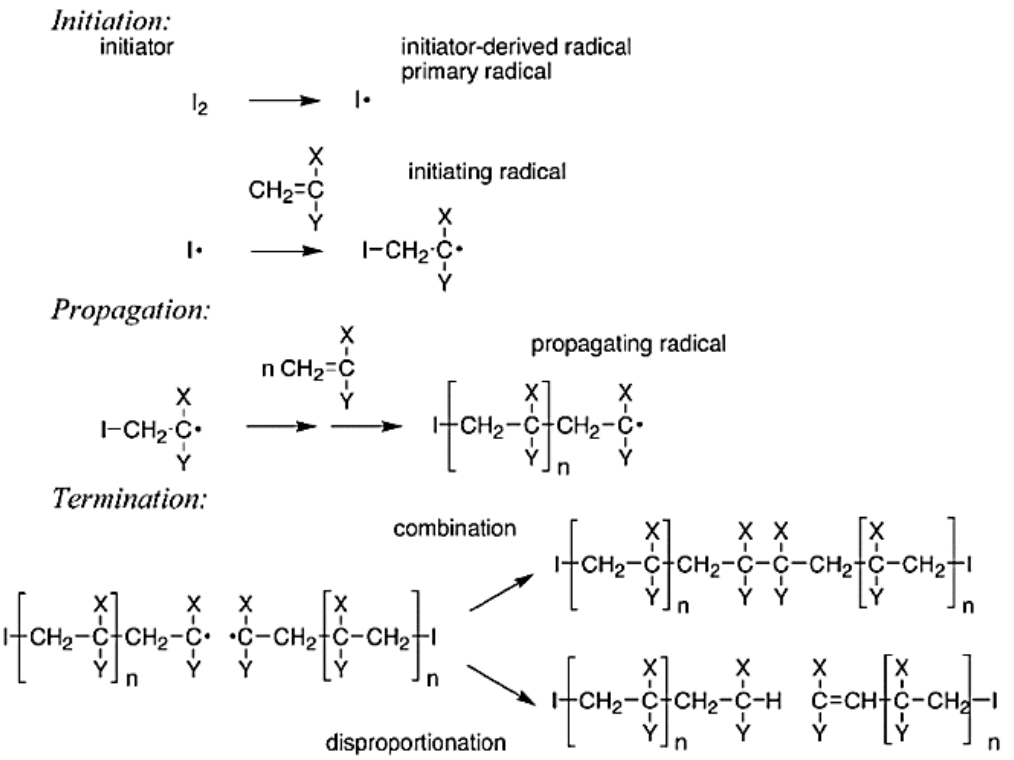

Figure 9 *Schematic representation of FRP mechanism with the step of activation, propagation and termination.*

In addition to this, many other termination reactions are possible, such as that of disproportionation, and that of transfer, in which the chain bearer reacts with the various chemical species present in the system, producing more or less reactive radicals.

1.5 GOLD NANOPARTICLES - HYDROGELS HYBRIDS

Recently it has been report a detailed study based on the work of Contreras-Caceres and his colleagues[15] that concerns the oxidation of spherical gold nanoparticles (GNPs) encapsulated into thermo- and pH-responsive microgels. Initially, two types of hybrid systems structured as 50 nm spherical gold nanoparticles coated with a thermo-responsive (N-Isopropylacrylamide) or a pH-responsive (4-vinylpyridine) microgel are synthesized. Then, a gradual gold elimination is achieved introducing each nanohybrid system into a mixture of cetyltrimethylammonium bromide (CTAB) and gold chloride (HAuCl4), finally obtaining hollow colloidal structures with potential application in controlled drug release. The synthesis of Au@pNIPAM and Au@p4VP systems is performed at

different crosslinking densities (5, 10 and 15%), and the decrease in the gold plasmon absorption band with the oxidation time is monitored at the two possible microgel states (swollen and collapsed).

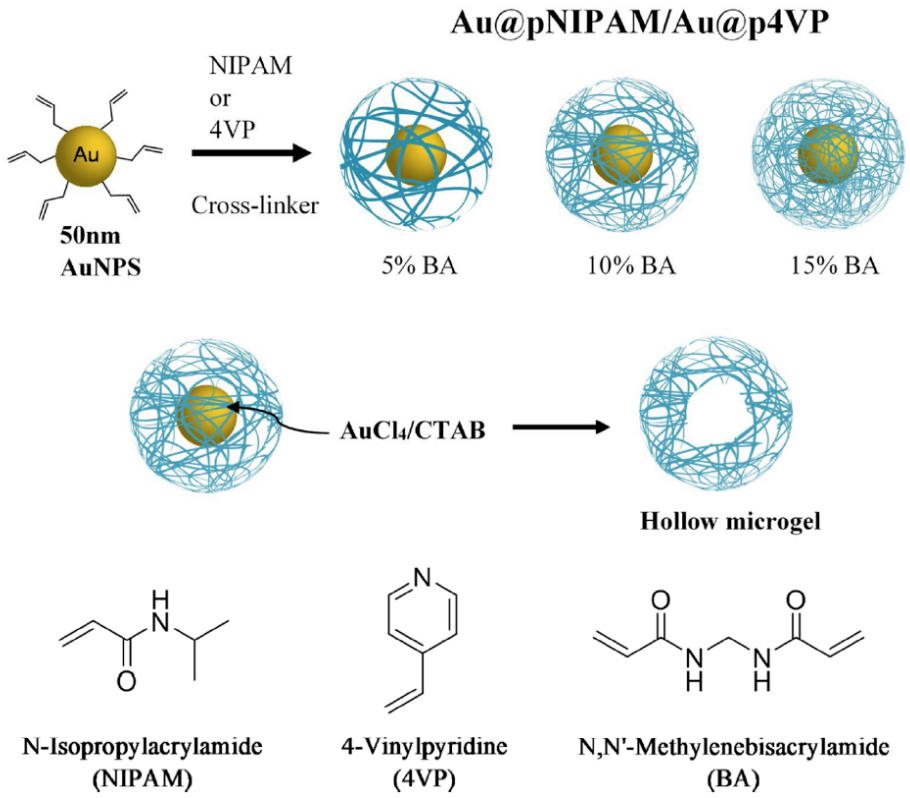

Figure 10 *Schematic representation for the synthesis of Au@pNIPAM and Au@4 V P microgels using 5, 10 and 15% BA (up). Au core oxidation and fabrication of hollow microgels.*

The described work, show the interesting possibility for the fabrication of hybrid microgels with tunable accumulation or release capability that may be applied in biomedical applications in in temperature controlled catalysis. More importantly, the fabricated hollow microgels can be used as microcontainers for the transport and delivery of biological specimen in nanomedicine.[16]

In fact, the fabrication of hollow colloidal structure at the nanoscale level is a promising method for encapsulation of different molecules or in our case for the formation of a catalytic site. Respect to traditional drug delivery systems, as vesicles, liposomes, or micelles, nanogels are much more stable and show a high degree of flexibility and moreover they have the capability to respond to changes in the external environment. This characteristic allows the system to exist in two different states, swollen and collapsed.

In this work[10] they investigate two types of polymers and their characteristics, poly (N-Isopropylacrilamide) (pNIPAM) and poly (4-vinylpyridine) (p4VP). They chose these two monomers, because possess thermo- and pH- responses capabilities.

1.5.1 Poly (4-vinylpyridine)

Poly (4-vinylpyridine) is a functional monomer. Concerning p4VP it has a phase transition state at pH-4.8. [17]Below this value the nitrogen atom in pyridine groups are protonated and for the repulsive electrostatic forces, so nanogels swell. Above that pH value instead the protonated nitrogen is neutralized and for the contribution of the vinyl group provides a collapse nanogel. [18]

4-Vinylpyridine (4VP)

Figure 11 *4-vinylpyridine monomer.*

1.5.2 Poly (N-Isopropylacrilamide)

The most extensively studied thermoresponsive polymer is poly-(N-isopropylacrylamide).

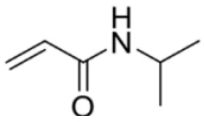

N-Isopropylacrylamide (NIPAM)

Figure 12 *N-Isopropylacrilamide monomer*

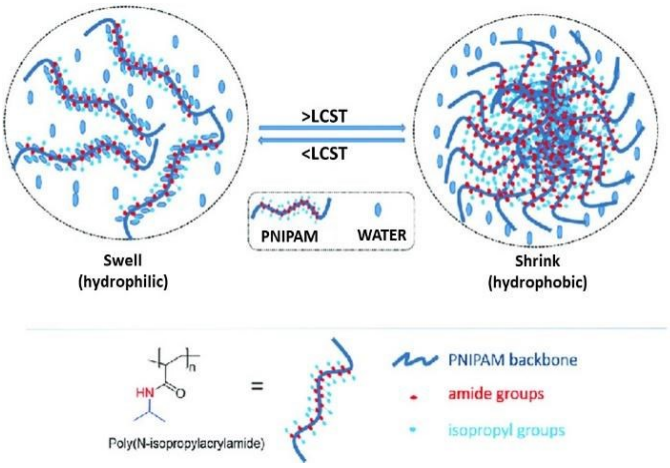

Figure 13 *Graphical representation of p-NIPAM behavior depending on LCST.*

It has a volume phase transition temperature at about 32°C in water. Below this temperature nanogels network form hydrogen bonds between acrylamide groups and water molecules, so it results in a swollen state. [19]

Above 32°C hydrogen bonds are broken, and hydrophobic forces takes water molecules out of nanogels, so the system collapse. The conformational change to a globule form buries most of the amide groups, which releases a significant amount of water, and hides the hydrophilic groups and exposes the hydrophobic ones, respectively. This process is reversible and by lowering the environmental temperature below the LCST. Below this temperature nanogels network form hydrogen bonds between acrylamide groups and water molecules, so it results in a swollen state, pNIPAM chains extend to their coil form, rehydrate and regain solubility and wettability. [20]

1.6 ALDOL REACTIONS

The aldol reaction is one of the most important C-C bond-forming reactions. It involves two carbonyl compounds as reactants, one acts as the latent enolate and the other serves as the electron sink, for the formation of β-hydroxy carbonyls.[21]

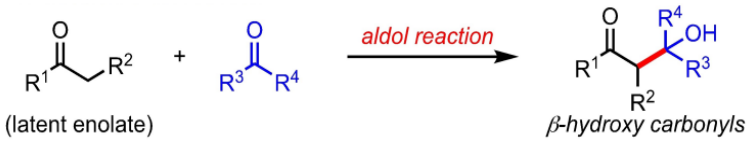

Figure 14 *The classical mechanism of aldol reaction.*

The synthetic potential of the aldol reaction has been demonstrated over several decades in the formation of many structurally challenging organic molecules. Because of the amount of biologically active compounds containing β-hydroxy carbonyl motifs, considerable efforts have been dedicated to develop chemo-, regio- and stereoselective versions. In fact, the stereochemical principles related to aldol reactions, its application in the context of total synthesis of natural products and the catalytic asymmetric aldol reactions have been weighed up so minutely that the evolution of the organic chemistry from its beginning to the recent state of the art can be viewed through the lens of the aldol reaction and its variants. [22]

A lot of enzymatic transformations have a synthetic counterpart. Often though, the mechanisms by which natural and synthetic catalysts operate differ a lot. The catalytic asymmetric aldol reaction as a fundamental C−C bond forming reaction in chemistry and also biology is an interesting case in this respect. Chemically, this enzyme-mediated reaction is dominated by approaches that utilize preformed enolate equivalents in combination with a chiral catalyst. Typically, a metal is involved in the reaction mechanism. A lot of enzymes, however, use a fundamentally different strategy and catalyze the direct aldolization of two unmodified carbonyl compounds. Class I[21] aldolases utilize an enamine based mechanism, while Class II aldolases mediate this process by using a zinc cofactor. In 1998 it was discovered the first small-molecule asymmetric class II aldolase mimics have been described in the form of zinc, lanthanum, and barium complexes. However, amine-based asymmetric class I aldolase mimics have not been described in the literature.

1.6.1 Aldol reaction Proline catalyzed

Importantly, in 2000[23,24] it was proposed that the amino acid proline is an effective asymmetric catalyst for the direct aldol reaction between unmodified acetone and a variety of aldehydes.

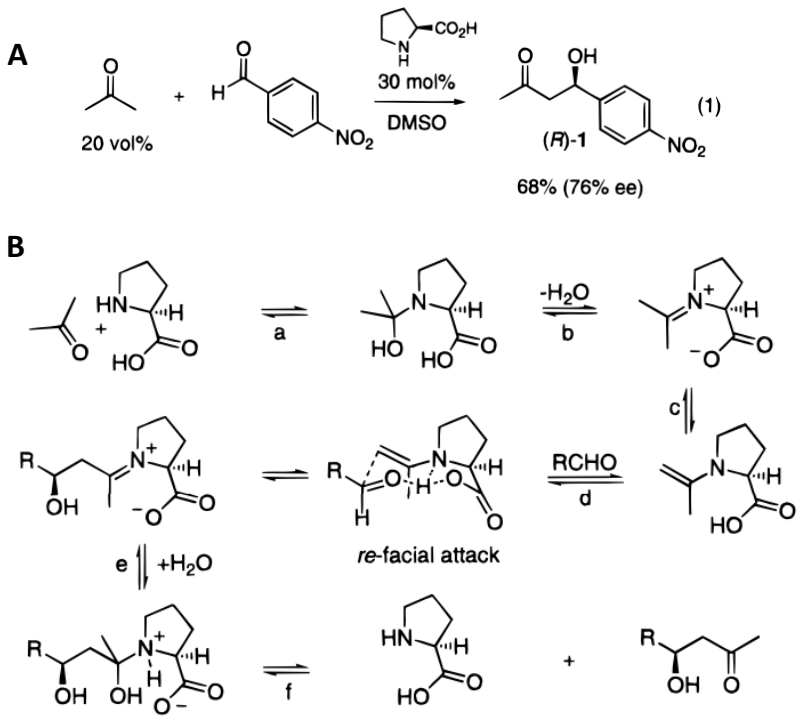

Figure 15 *Proposed Enamine Mechanism of the Proline-Catalyzed Asymmetric Aldol Reaction.*

Currently,[25] it is still assumed that this aldol reaction occurs via an enamine mechanism (Figure 15). Proline, acts as a "micro-aldolase" [26] that provides both the nucleophilic amino group and an acid/base cocatalyst in the form of the carboxylate. This co-catalyst may facilitate every individual step of the mechanism, the nucleophilic attack of the amino group (a), the dehydration of the carbinol amine intermediate (b), the deprotonation of the iminium species (c), the carbon−carbon bond forming step (d), and both steps of the hydrolysis of the iminium-aldol intermediate (e and f). The tricyclic hydrogen bonded framework provides for enantiofacial selectivity.

2 MATERIALS AND METHODS

2.1 REAGENTS AND SOLVENTS

Carlo Erba	ACN per HPLC
Fluka	NaCl
	Nitrobenzaldehyde
	Acetone
	Cicloexanone
	DIPEA
Euriso-Top	Deuterated chloroform
Honeywell	Boc-L-Proline
Merk	KHSO4
	NaHCO3
	NaCt
	Anhydrous sodium sulfate
SigmaAdrich	AcOEt
	BSA
	EDC
	TFA per HPLC
	TFA ReagentPlus
	$HAuCl_4$
	NaCt
	N-isopropylacrilamide
	N-N methylenbisacrilamide
	2,2′-azobis(2-methylpropionamidene) dihydrochloride

2.2 EQUIPEMENTS

2.2.1 UV- spectroscopy

The acquisition of the absorption spectra in the UV-Vis field is done with a Shimadzu UV-2501PC spectrophotometer. Such instrumentation covers a range that goes from 190 to 900nm through the use of a double monochromator, one for low wavelengths and one second for high wavelengths. The detector is an R-928 photomultiplier.

2.2.2 High-Performance Liquid Chromatography.

The HPLC measurements were performed using an Agilent 1200 apparatus (Palo Alto, CA), equipped with a UV detector at various wavelength and a column Agilent extend-C18 (stationary phase). Eluants: A= 9:1 H_2O/CH_3CN, 0.05 % TFA; B= 1:9 H_2O/CH_3CN, 0.05 % TFA.

2.2.3 Circular Dichroism

The tool used for DC analysis is Jasco J-1500. The cuvette is made of quartz with an optic path of 0.1 cm. It works in the UV region and in the infrared district.

2.2.4 Nuclear Magnetic Resonance.

^{1}H NMR, ^{13}C NMR, and 2D-NMR spectra were recorded at 25°C on Bruker Avance400 or 500 MHz instruments. ^{1}H and ^{13}C spectra were referenced relative to the solvent residual peaks and chemical shifts (δ) reported in ppm downfield of tetramethylsilane ($CDCl_3$ δ H: 7.26 ppm, δ C: 77.16 ppm; CD_3CN δ H: 1.94 ppm; DMSO δ H: 2.50 ppm). The multiplicity of a signal is indicated as br, broad; s, singlet; d, doublet; t, triplet; m, multiplet.

2.2.5 Transmission electron microscopy

The images acquired through TEM (Transmission Electron Microscopy) were made by using the FEI TECAI G12 instrumentation, which uses a tungsten wire as a source of electrons for the thermionic effect. Liquid samples that have been

observed with this type of transmission electron microscope are prepared by placing a drop of the highly diluted sample solution onto a 400 mesh copper screen covered with a carbon film, which acts as a support

(Acquisitions made in the Department of Biology)

2.2.6 Dynamic Light Scattering

DLS measurements were made with one Malvern's ZetaSizer NanoS instrument using a laser operating at 633 nm e measures the intensity of diffused light at 176°. Cuvettes in plastic with an optical path of one centimeter in thermostated cell holders with a Peltier system

2.3 GOLD NANOPARTICLES SYNTHESIS.

Gold nanoparticles synthesis is based on Turkevich method. It provides an aqueous solution containing Gold (III) chloride hydrate that is reduced using a solution of trisodium citrate (NaCt). It starts using a round-bottom flask and an hotplate. We make a stock solution, adding first 100 ml of Deionized water (MΩ), and then 50 mg of $HAuCl_4 \cdot 3H2O$ (339.785 g/mol + 54.045 g/mol; 0.128 mmol)

Then we prepare, independently a Sodium citrate diihydrated solution ($NaCt \cdot 2H_2O$) (258.06 g/mol + 36.03 g /mol; 0.5 mmol) in 10 mL of water.

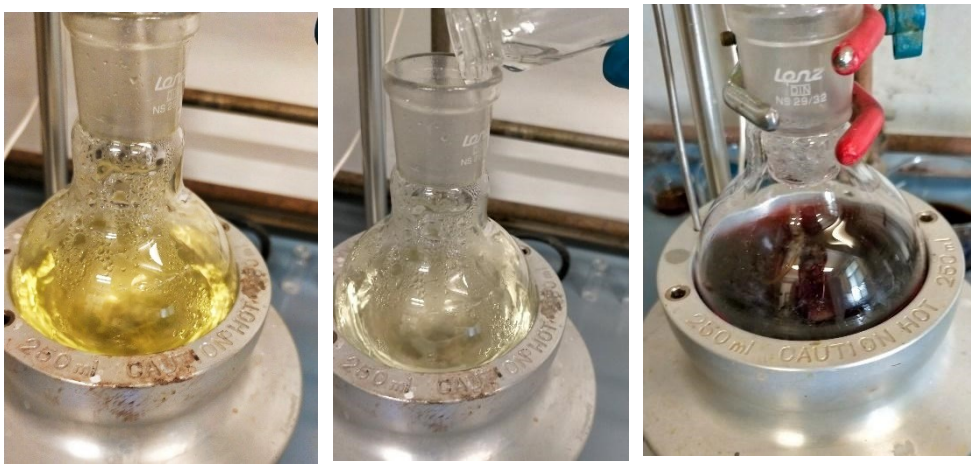

Figure 16 *Gold nanoparticles synthesis process. In the first image yellow solution is only HAuCl; in the second one is just after NaCt addition; the third image is when process is going to finish.*

The flask containing $HAuCl_4$ solution is heated gradually until reaching a temperature of 120°C. In order to avoid evaporation a bubble refrigerator is set up over the flask. When solution reaches boiling point NaCt solution is rapidly added to $HAuCl_4$ solution, under a vigorous stirring. The initial solution is yellow, after reductant addition it becomes transparent, then becomes black and at the end deep red. The reaction took 20 minutes and it is complete when solution color no longer changes.

Dialysis is used to purify nanoparticle, to purify from salts i.e. sodium citrate . Dialysis membrane is made to swell with deionized water. When membrane is hydrated, one end is closed with a clip. After solution is put inside membrane, another clip is used to close the other end. Membrane is put inside a baker fill of water overnight. Dialysis is preferred to centrifugation, to avoid excessive nanoparticles aggregation and precipitation.

Nanoparticles solution is stored in the dark at 5°C.

2.3.1 50 nm GNPs synthesis.

First the initial stock solution of GNPs is diluted in 50 ml of water. Then we have prepared a "growth solution", an aqueous solution, with 200 µL of $HAuCl_4 \cdot 3H_2O$ and 50 mg of $NaCt \cdot 2H_2O$.

2.4 NANOPARTICLES STABILITY WITH BSA.

In this experiment we have tested nanoparticles stability in different condition of osmolarity, to mimic harsh environmental conditions. To change ionic strength we have used different amount of Sodium chloride (NaCl). Change of stability has been shown with UV-spectrum. Enhancing ionic strength, nanoparticles gradually aggregate and precipitate, but they show a different behaviour when there is a protein layer on their surface. It is possible to demonstrate this phenomenon with two experiment:

1° experiment: Nanoparticles solution at different NaCl concentrations. UV spectra were taken adding 10 µL of NaCl 10 mM for every measure.

2° experiment: Nanoparticles with BSA monolayer in NaCl solution.

The same nanoparticle solution from the previous experiment is incubated with BSA solution (0.0003 mM). As made before for every UV measure 10 μL of NaCl 10mM are added.

2.5 BSA FUNCTIONALIZATION WITH L-PROLINE.

2.5.1 BSA functionalization with Boc-Proline-OH.

In a round-bottom flask is weighted 200 mg of BSA and it is dissolved in 10 mL of H2O Mq,

In another random-bottom flask it is necessary to prepare the other reactants to make peptide bond between Boc-Proline and Lysine residues of the protein. In a volume of 4 mL of acetonitrile are added:

- 500 mg of Boc-Proline (MW = 215.25 g/mol);
- 270 mg of N-hydroxysuccinimyde (MW= 115.09 g/mol);
- 444 mg of 1-Etil-3-(3-dimetilamminopropil)carbodiimmide, EDC (MW= 155.24 g/mol.

Reaction course is controlled with HPLC analysis.

Then rotavapor is used to remove acetonitrile from product. Boc removal is got adding:

- 10 mL of Trifluoroacetic acid (TFA);
- 2 mL of water.

Also in this case, TFA is removed by rotavapor, then sample is freeze-dried. From this reaction we have obtained 156 mg of modified BSA. At this point BSA is incubated with GNPs solution

2.5.2 BSA functionalization with Proline NCA.

2 gr of Boc-L-Pro-OH (0.009) mol were dissolved in 20 ml of CH_2Cl_2. To this solution 2 gr of oxalyl chloride (0.05 mol) were added, follow by the addition of

three drop of anhydrous DMF. The reaction was allowed under stirring for 3 hrs. Solvent was removed under reduced pressure. The resulting crude, was taken with ethyl acetate, and the organic layer was washed two time with a $NaHCO_3$ saturated solution, and finally with brine. The organic layer was treated with anhydrous Na_2SO_4, filtered and removed in vacuum. Pro NCA was obtained in 65 % yield as a withe solid. [27]

An aqueous solution of BSA (0.3 mM) is prepared under magnetic stirring in a volume of 5 mL of water. To maintain a basic pH, 1 mg of sodium bicarbonate (NaHCO3) is added to the solution.

Proline NCA is diluted in 2 mL of Acetonitrile (CH_3CN). This solution is added in two times spot, under magnetic stirring at 37°C:

- T1 → 100 µL of Proline;
- T2 → 200 µL of Proline.

Reaction course is controlled through HPLC analysis. After characterization sample is dialysate for one night and then freeze-dried.

2.6 BSA-PRO PROTEIN CORONA FORMATION AROUND GNPS.

At this point one time that BSA has been modified, 20 mg of BSA-Pro (0.3 mmol), are dissolved in 2 ml of water (0.15 mM).

5 mL of GNPs are put in a round bottom flask and incubated, with 1 mL of the previous solution. It is necessary to add the protein solution slowly, possibly drop by drop, to avoid protein aggregation. After about 30 minutes, 1 mL of the BSA solution is added again so to improve protein corona formation and realize an hard corona on GNPs surface.

2.7 2.3.2 GNPS-(BSA-PRO) FUNCTIONALIZATION WITH FLUORESCEIN ISOTHIOCYANATE.

GNPs with L-Proline-BSA layer is put in a round-bottom flask and under magnetic

stirring is incubated with 2 mg of fluorescein isothiocyanate (FITC) (389.38 g/mol; 0.005 mmol).

After the reaction is let go on for 30 minutes at room temperature, then it is centrifugated at 4500 rpm to remove FITC. In fact supernatant is yellow, so contain FITC that has not react. Pellet is storage, redispersed and centrifugated again.

2.8 BSA FUNCTIONALIZATION WITH BUTANOIC ACID.

BSA functionalization with Butanoic acid occurs incubating previous product, 220 mg of EDC in 4 mL of water for acid carboxylic activation. When EDC is dissolved 200 μL of Butanoic acid are added (86.09 g/mol). Reaction is stopped after 20 minutes.

Then is centrifugated at 4500 rpm for 30 minutes. Pellet is redispersed in a volume of 5 mL of water and the centrifugated again. Pellet is isolated from supernatant and dispersed in 5 mL of water and storage.

2.9 POLYMERIZATION

Functionalized nanoparticles are redispersed in 50 ml of 4mM CTAB. The excess of butanoic acid is removed by centrifugation at 4500 rpm for 30 minutes. The supernatant is discarded and pellet is redispersed in 10 ml of water with 125 μL 5m CTAB.

5 ml of this solution is put in a random-bottom flask, and is heated to 70°C. In order are added:

- 0.070 g of N-isopropylacrilamide monomers (NIPAM)
- 0.010 g of bisacrylamide (BA) (154,17 g/mol)
- 50 μL of 2,2′-azobis(2-methylpropionamidene) dihydrochloride (V50), (271,19 g/mol) concentration of 0.1M.

After 3-4 minutes red solution becomes turbid, and reaction is allowed to proceed for 2 hours at 70°C.

After this period polymerization is stopped and solution is allowed to cool to room temperature, under stirring.

Then it is diluted with 50 ml of water and centrifugated at 4500 rpm for 30 minutes, in this way it is possible to separate nanogels from reagents that have not react. The pellet contains nanogels. Supernatant is discarded; the pellet is diluted and centrifugated again. This operation is allowed to proceed for a couple of times, to have a good sample. At the end of last centrifuge, pellet has been dispersed in 5 mL of water.

Figure 17 *Solution of GNPs after polymerization process.*

2.10 ETCHING

Gold core oxidation has been achieved following literature procedure[28]. First a solution of CTAB/ $HAuCl_4$ has been prepared. $HAuCl_4$ concentration is 0.275 mM, is added to a CTAB solution of 100 mM in a volume of 5 ml of water. The previous solution of GNPs-pNIPAM nanogels is heated at 50 °C and the CTAB/HAuCl solution is added rapidly. Reaction is allowed to go on for about 30 minutes, during while purple solution becomes gradually transparent. One time that is stopped, it is allowed to cool at room temperature. Also these time is necessary to make three centrifugations to separate hydrogels just formed, which are in the pellet, and gold ions which are in the supernatant part. Centrifugation are made at 4500 rpm for 30

minutes. The final pellet obtained from the final centrifugation is dispersed in 5 mL of water and storage at 5°C.

Figure 18 *Solution of pNIPAM nanogels after gold core oxidation.*

2.11 SOLID-PHASE SYNTHESIS.

The aldolic reaction catalyzed by gold nanoparticles decorated with the dipeptide Cysteine-Proline[29], is used as control reaction to see the product formation and to compare this to the one catalyzed by BSA-Pro. In the review they do not specify how to make the dipeptide so we have decided to use solid-phase peptide synthesis.

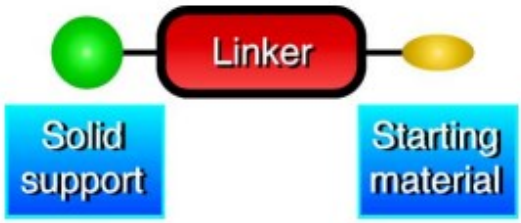

Figure 19 *Schematic representation of molecule immobilization on the polymeric support.*

Solid phase synthesis of peptide is based on the elongation of aminoacidic sequence while it is anchored to a solid support. The main advantage of this technique is that is easy to remove reagents and solvents from the peptide. The solid support is a resin, which is inert and insoluble.[30] It has specific functionalization that allow the immobilization of the first molecule on the resin. Then is necessary a linker to attach

the small molecule on the resin. Peptide growth starts with the C-terminal amino acid and proceeds to N-terminal. The reaction of coupling between the two amino acids is a condensation, between the amine group of the C-terminal residue and the carboxylic group of the N-terminal residue. Is necessary to protect the amine group of the second amino acid to guarantee that this one reacts with the one just present.

The protector groups used in this experiment are: Boc group to protect amine function of Proline, Fmoc group to protect amine group of Cysteine, and Trityl group which protect the sulphur of Cysteine. [31]

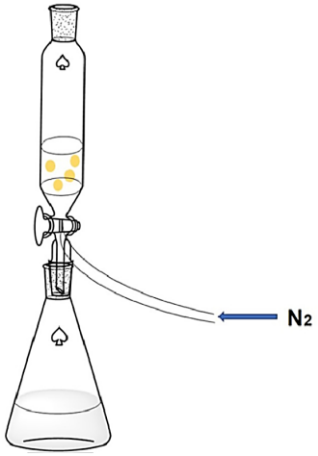

Figure 20 *Graphic representation that describes the reactor used for solid-phase peptide synthesis.*

We have used 3 g of 2-chlorine trityl resin, that must be swelled with 15 mL of Dimethyl sulfoxide (DMF). The entire process takes place in a small reactor which has two exit, one for solvents flux, and one for nitrogen flux. Every passage needs to be under nitrogen flux to guarantee a continuous mixing. The bond between the resin and Cysteine is made preparing a solution with 2.46 g of Fmoc-Cys(Trt)-OH and 700 µL of N,N-Diisopropylethylamine (DIPEA) in 15 mL of DMF. The reaction is let to go on for 1 hour. After this we make a wash with DMF, and the with a solution which contain DCM, MeOH and DIPEA (80:15:5). We let stir it under N flux for 20 minute. The resin is washed three times with DCM and then three times with DMF.

At this point there is the deprotection step of Cysteine, with Fmoc remotion. We add to the reactor a solution of PIP at 20% in DMF for 20 minutes. After this time

we make a wash with DMF and the process with PIP is repeated. After resin is washed with DMF, DCM and at least with DMF, there is coupling step.

We prepare a solution containing 2.5 g of Boc-Pro-OH, 4g of HATU and 163 mg of HOAt, in a volume of 15 mL of DMF and 2 mL of DIPEA. Coupling can stay for 1 hour after continuous nitrogen flux. Then resin is washed with DMF and then with DCM to dry the resin and remove DMF.

At this point the peptide must be detached from the resin. In the reactor we add a solution containing DCM and hexafluoroisopropanol (7:3) and let standing for 1 hour. This procedure is repeated another time and at the end the resin is discharged in a flask and dried to obtain the solid product. We have obtained 1.400 g of product.

Now we use a thin layer chromatography (TLC) to visualize the product and separate it from the by-products. The eluent used is a mining of DCM and MeOH (95:5). Purification is obtained using a silica column with the same eluent of TLC. The product is collected in a round bottom flask and dried with rotavapor.

The deprotection of the two residues happens simultaneously, with a solution containing TFA, DCM and TIS. Solution becomes red. Reaction is followed with TLC. The solution is dried with rotavapor. Deprotection of Trt is executed washing solution with water, because peptide is soluble in water, while Trt not. Then solution is filtered and freeze-dried. So at the end we have obtained 1.200 g of product, that can be used to decorate GNPs.

3 RESULTS AND DISCUSSION

3.1 NANOPARTICLES SYNTHESIS

As described in previous chapters the creation of these nanogels is a step process, composed by different pieces that have been characterized. First step is gold nanoparticles synthesis with Turkevich method. We have characterized nanoparticles formation with UV-spectroscopy and TEM images.

In the graph in figure 22 it is possible to see maximum absorption at 519 nm. The intensity and position of surface plasmon oscillation peak are related to various parameters. In this case, shape symmetry and also the fact that peak width is narrow indicate that colloidal gold has good monodispersity and spherical shape. The term monodispersity is related to a cluster of objects that have approximately the same size and shape.

This feature is visible in the TEM image of GNPs (Fig. 21). Looking at the scale it is possible to measure nanoparticles diameters, it is in a range of 15-20 nm; and about shape, most of them are spherical, but it is possible to observe the presence of interesting shape, triangular for example. For our aim, we have assumed that spherical shape would be the best choice.

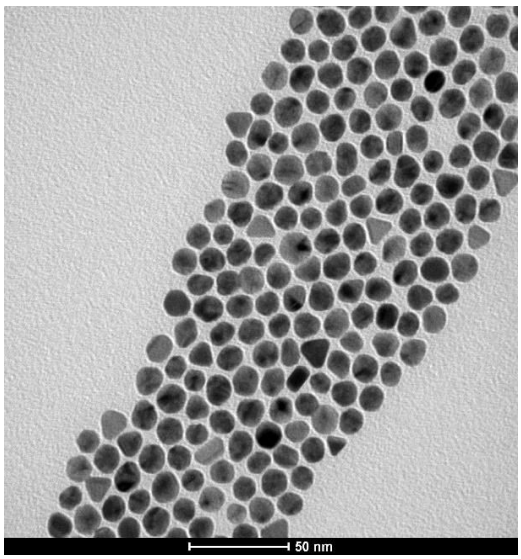

Figure 21 *TEM image of GNPs solution*

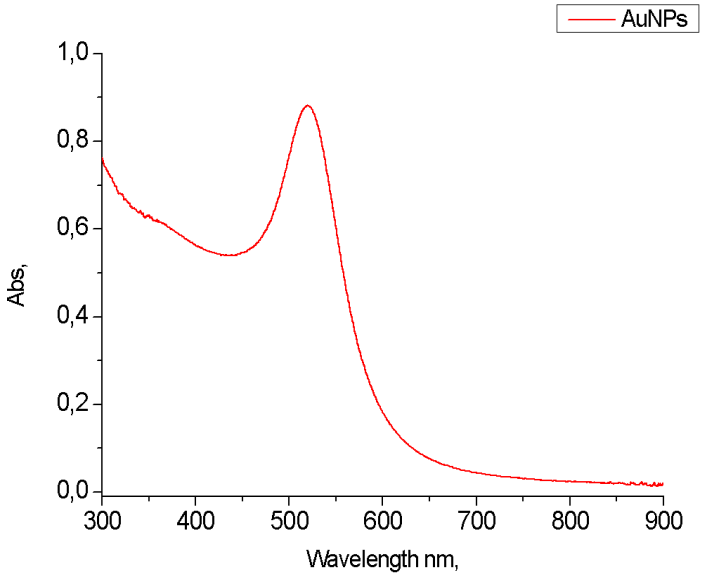

Figure 22 *UV-spectrum of GNPs solution. The peak at 519 nm is given by surface plasmon.*

Thanks to Dynamic Light Scattering measures we have a precise size distribution value of nanoparticles size. DLS gives information about the light scattered by the objects present in the sample. DLS uses thermal energy of particles in suspension which move with a Brownian motion. When in solution, nanoparticles move randomly in all directions and they collide with solvent molecules. These collisions take to have a certain energy which induces NP movement. There is a relationship between particles movement speed and their size that is described by the Stokes-Einstein equation. [32] In the equation "D" is diffusion coefficient, "Kb" is Boltzmann constant, "T" is temperature, "η" is viscosity, "Rh" is the hydrodynamic radius.

$$D = \frac{\mathrm{KbT}}{6\pi\eta\mathrm{Rh}}$$

From this equation the system is able to give as output the hydrodynamic radius of every NP.

In the graph below there is also the term (PDI) which stands for polydispersity index and this value describes the broadness of particle size distribution. When this value is in a range between 0 to 1 the distribution in quiet monodisperse.

Instead Z-Average Diameter is the intensity weighted mean hydrodynamic size derived from the cumulant analysis; it depends a lot by aggregates presence or contaminants presence.

From this first GNPs sample we have obtained a single peak so the sample in monodisperse and the average diameter is 20.86 nm.

			Size (d.n...	% Number	Width (d.n...
Z-Average (d.nm):	103,8	Peak 1:	20,86	100,0	6,202
PdI:	0,277	Peak 2:	0,000	0,0	0,000
Intercept:	0,930	Peak 3:	0,000	0,0	0,000
Result quality	Good				

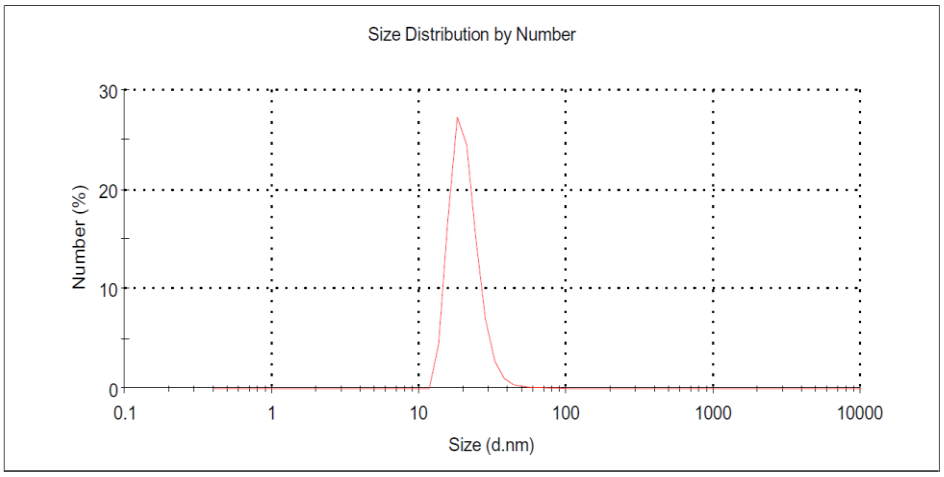

Figure 23 *Size distribution of GNPs with DLS measures.*

There are works that describes very well how nanoparticles size and diameter depend on molar ratio of the reagent mixture, and temperature too. [33]

For this reason we have tried to synthetize bigger nanoparticle[15] as shown in the figure 24. The procedure essentially follows Turkevich synthesis. It starts from GNPs stock solution with a diameter of ~15 nm, this is the "seed solution". A "growth solution" is prepared, in this case the difference is the absence of butanoic

acid, which is essential for the vinyl termination. In this aqueous solution there are all the other reagents, so $HAuCl_4$ and NaCt.

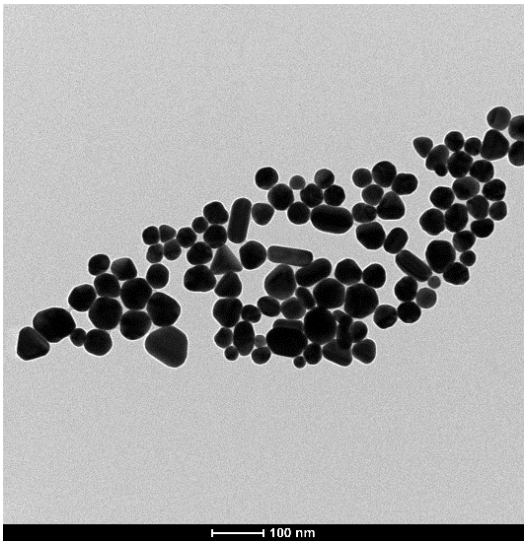

Figure 24 *TEM images of growth GNPs.*

In this image obtained by TEM, it is evidence the difference respect to the stock nanoparticles, average diameter is about 50 nm. Moreover, GNP sample becomes more polydisperse, there are nanoparticle with different diameter and various shape, not only spherical, but also triangular and nanorods. Also DLS measures confirm this. In fact, respect to the peak in Fig. 23, this peak is larger, and also PDI value is bigger than the first sample. So, the sample is not monodisperse there is more inhomogeneity.

			Size (d.n...	% Volume	Width (d.n...
Z-Average (d.nm):	68,84	**Peak 1:**	51,42	100,0	36,34
PdI:	0,282	**Peak 2:**	0,000	0,0	0,000
Intercept:	0,884	**Peak 3:**	0,000	0,0	0,000
Result quality	Good				

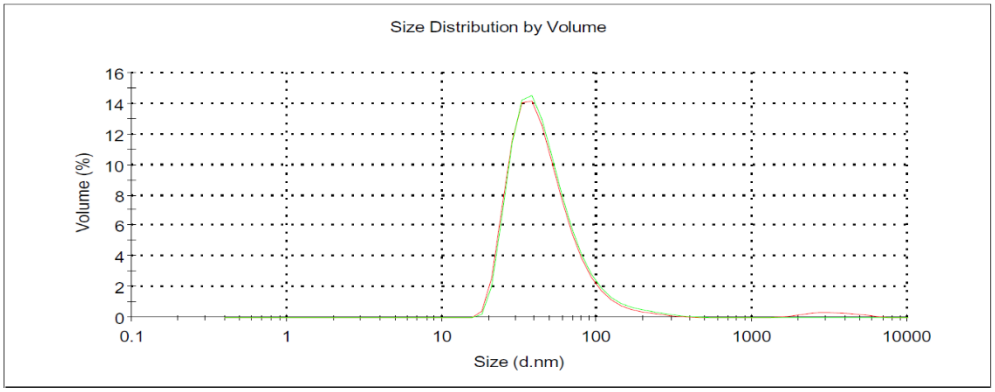

Figure 25 *Size distribution of growth GNPs with DLS measures.*

For this reason in this case, we have proceed the other experiments following the initial protocol, to have a batch solution with precise characteristics.

3.2 BSA PROTEIN CORONA ON GNPS SURFACE

BSA interaction with 20 nm GNPs surface has been investigated with three methods.

By UV-spectroscopy, in presence of BSA, GNPs plasmonic peak has a red-shift and a broadening of absorption band. These changes indicate BSA adsorption on GNPs surface. Starting from the same sample of GNPs, four addition of BSA, at the same concentration (0.0003 mM), were made.

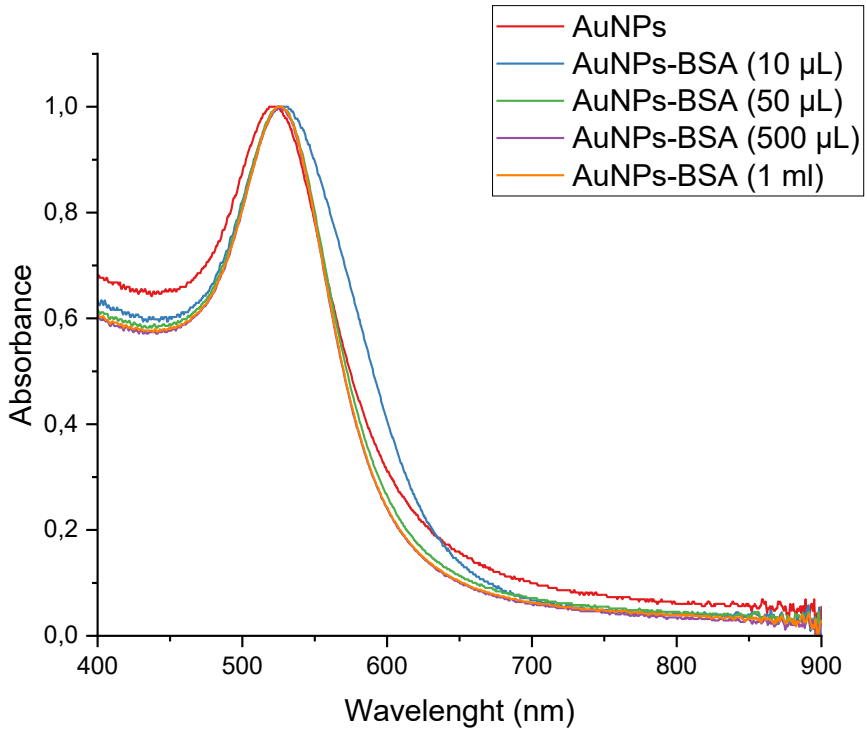

Figure 26 *UV-spectrum of same GNPs sample incubated with BSA at different concentrations.*

Sample	Wavelenght (nm)
AuNPs	519
AuNPs-BSA (10 µL)	523
AuNPs-BSA (50 µL)	252
AuNPs-BSA (500 µL)	526
AuNPs-BSA (1 ml)	530

Table 1 *Uv absorption shif after GNPs are incubated with increased BSA concentration.*

Below (Figure 27) there are TEM images of 50 GNPs incubated with BSA. In the first image protein corona is visible around nanoparticles, thanks to staining. In the second image there is the same sample but is without staining. By second figure it is possible to assume that BSA can stabilize GNPs, in fact nanoparticles are more dispersed and less aggregated.

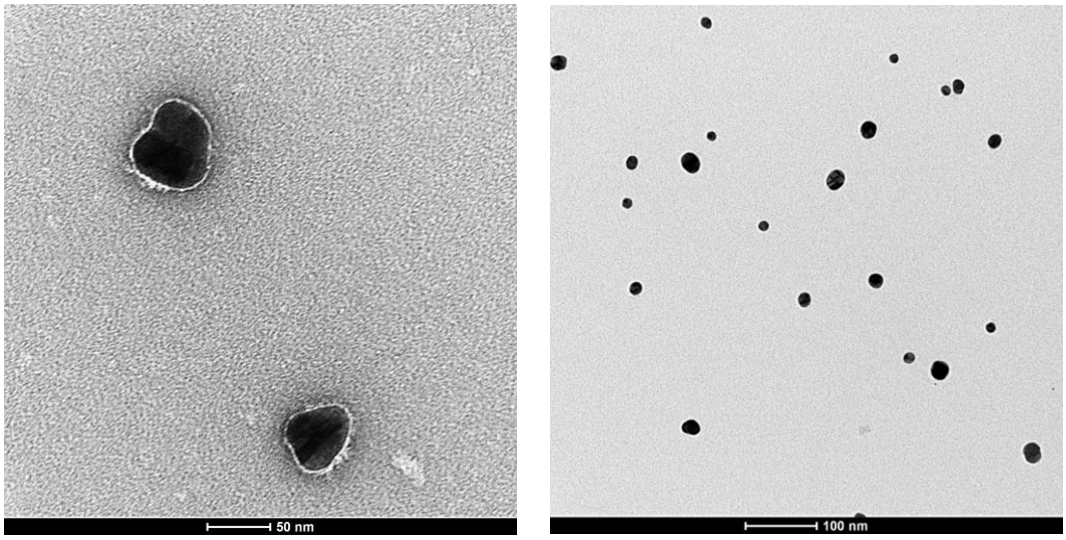

Figure 27 *TEM images of GNPs incubated with BSA.*

The main contribution on BSA conjugation with GNPs is given by the presence of non polar hydrophobic groups that act the main effect on the bindings of colloidal gold and serum albumins. In literature are reported various mechanism of interactions between BSA and GNPs. First of all, the electrostatic interactions between the positive charged lysine of the protein and the negative citrate layer covering NPs surface; then the particular stability of thiol-Au bond, given by cysteine residues. In particular Cys-34, which seems to be one of the major cause of "ligand exchange" , to displace citrate[34].

3.3 GNPs STABILITY

At this point we investigate how BSA can stabilize GNPs, until under aggregation condition. Generally, nanoparticles aggregate and precipitate in an aqueous solution that has a pH and ionic strength as human blood plasma. For this reason we have made two experiment using the same conditions, same pH, and same ionic strength.[34]

Nanoparticles aggregation and precipitation is optically visible, because solution gradually change his color, from red to violet and by UV-spectrum, given by plasmon coupling. The typical plasmonic peak of stabilized nanoparticle at 520 nm, has a large red-shift. This phenomenon is due to citrate anions interactions with Na+ cations in solution, that takes systems to collapse. The experiment is reported in fig. 29. It is clear visible that subsequential addition of incremental amount of NaCl affect the aggregation of the nanosystem as shown from the red-shift of the plasmonic band.

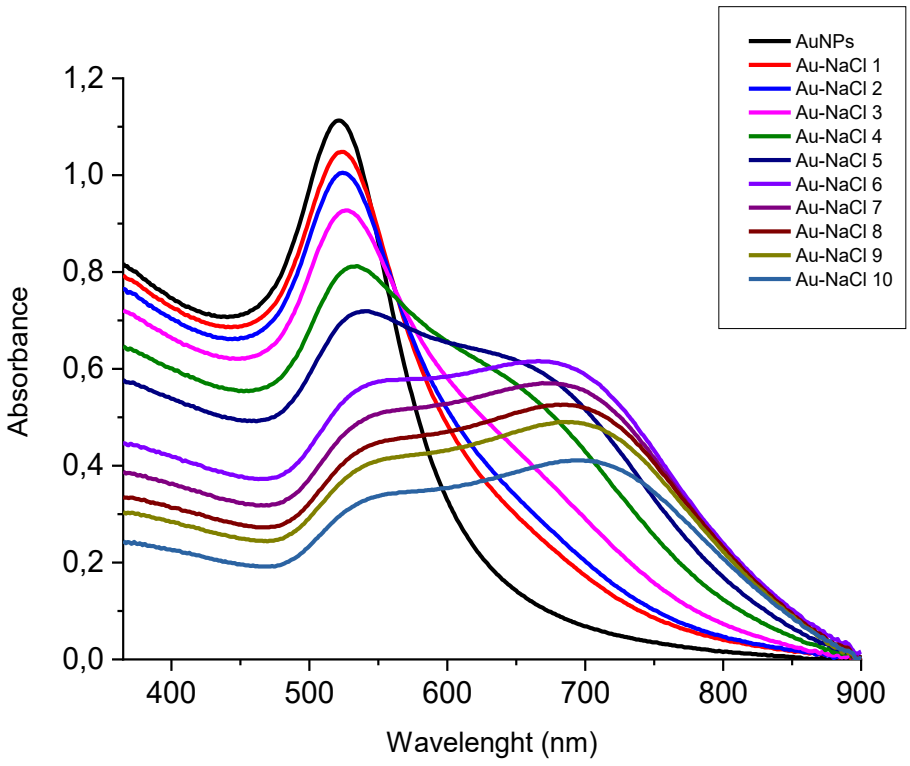

Figure 28 *UV-absorption spectrum of same GNPs sample but at increased ionic strength condition.*

The very same experiment has been repeated, after the GNPs At this point the experiment has been repeated, after that GNPs have been incubated with BSA (0.0003 mmol). As it can be seen from fig. 30, after the increase of ionic strength we do not see any change in plasmon resonance.

Thus BSA adsorption on nanoparticle surface enhances colloidal stability even when salt concentration increase.

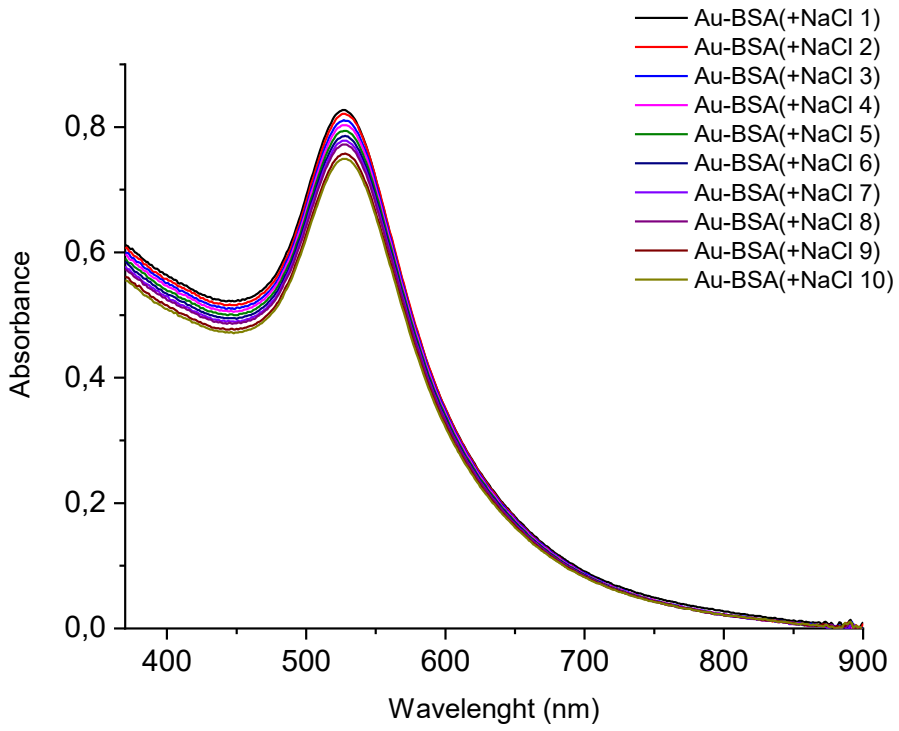

Figure 29 *UV absorption spectrum of GNPs-BSA at increased concentration of NaCl.*

This is an interesting result for the following step for nanogels formation. This means that we can use it as stable "scaffold" for the following steps, so for the other modifications, without the risk of nanoparticles aggregation and precipitation.

3.4 BSA MODIFICATION WITH L-PROLINE.

In the way to mimic proline as catalyst toward a stereoselective aldol condensation we plan to add chemically Proline to the Lys amine on BSA protein, which is classified as a polar basic amino acid for the ammine group presence. The novel protein is supposed to displayed comparable stereoselective capability than the

original proline. This because e may assume that the adjacent Asp and Glu residues along the primary sequence of BSA will give the required assistance of the carboxylic unit to the secondary amine of the proline, as occurring in the case of the single amino acid (Pro). BSA aminoacidic sequence contains 58 Lysine residues that are useful for our aim, to make a peptide bond with Proline.[8]

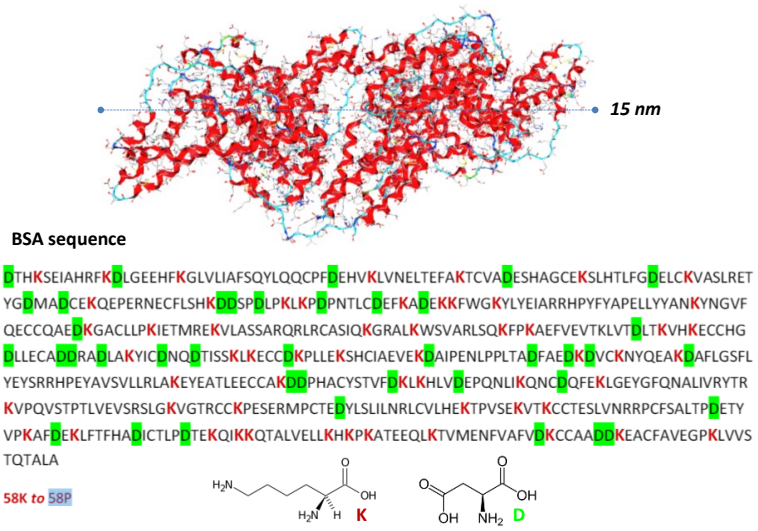

Figure 30 *BSA structure and primary amino acidic sequence.*

About 30-35 Lysine of BSA have primary amines that are capable of conjugation. When BSA is in aqueous solution is essential to have a basic pH, for this reason Sodium bicarbonate is added. A basic pH ensures to have protonated Lysine, so a good nucleophile. [36]

For peptide bond formation between Lysine and Proline, it is necessary to use Boc-L-Proline. Boc, which stands for terzbutil-oxy-carbonyl is a protector group, used to avoid amine group reactivity of the amino acid, transforming it in an amide.

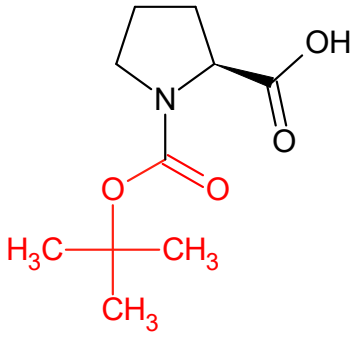

Figure 31 *Boc-Proline chemical structure. Boc group is underlined in red.*

The previous preparation of Boc-Proline with EDC and N-idroxysuccinimide, is fundamental to have the product Boc-L-proline N-hydroxysuccinimide ester (Boc-Pro-OSu). N-hydroxysuccinimide is used with EDC, a coupling reagent, and the amino acid of interest. NHS is widely used in the activation of carboxylic acids to NHS-esters to promote coupling with nucleophiles. There is the formation of acid intermediate very reactive. In this way Proline carboxylic group is activated and ready for the coupling with Lysine ammine group. Below there is a schematic representation of the mechanism of the reaction. (Fig. 32)

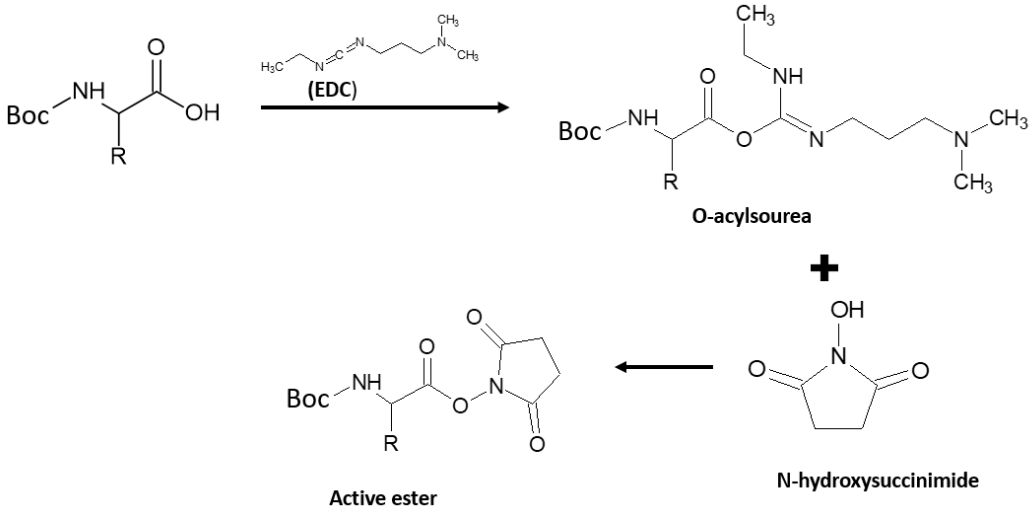

Figure 32 *Schematic representation of active ester formation from a Boc protected general amino acid.*

The final product, for Boc-L-Proline activation, is the molecule represented in figure 33:

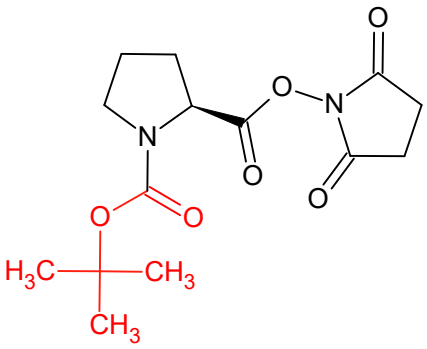

Figure 33 *Boc-L-Proline-N-hydroxysuccinimide chemical structure. The red structure is Boc.*

At this point, activators and byproducts are removed through a series of washes. First an acid one, with $KHSO_4$, then a basic wash with KOH and at least a neutral wash with Brine solution. The product is redispersed with ethyl acetate and dry with calcium phosphate, to remove every possible water molecule.

When this product is incubated with our protein, there is the coupling with Lysine residues. The evolution of coupling has been analyzed through HPLC analysis. We have used a C18 column.

To see BSA functionalization, it is necessary to inject every analytes. But to obtain the real product, it has been centrifugated, and both pellet and supernatant have been injected in HPLC. The difference in retention time (t_R) can help to distinguish the final product from the other reagents.

In the chromatogram below (Fig. 34) there is only BSA course dissolved in water. t_R is 6.696.

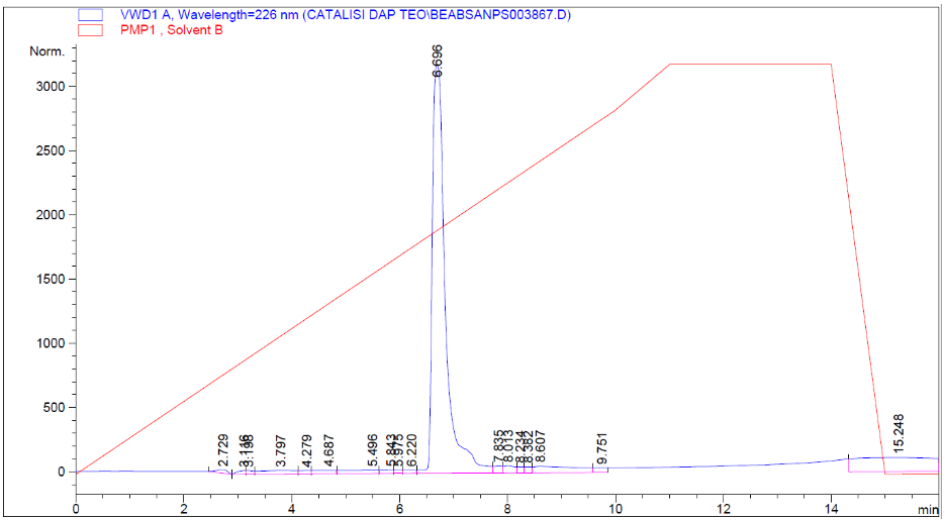

Figure 34 *BSA chromatogram.*

For the second reagent, so Boc-L-proline N-hydroxysuccinimide ester, there are two peaks. The first one which has a t_R of 2.772 is N-hydroxysuccinimide that hasn't still react, while the second one with a t_R of 7.935 is the ester.

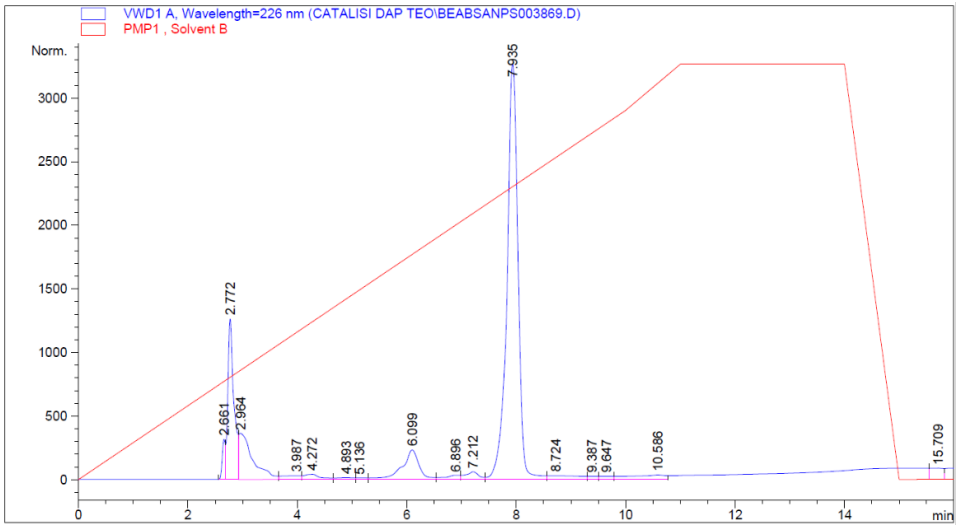

Figure 35 *Boc-Pro-OSu chromatogram.*

The chromatogram in figure 36 is referred to supernatant. The first peak at 2.850 is N-hydoxysuccinimide. The second peak at 8.870 could be BSA, the product or Proline.

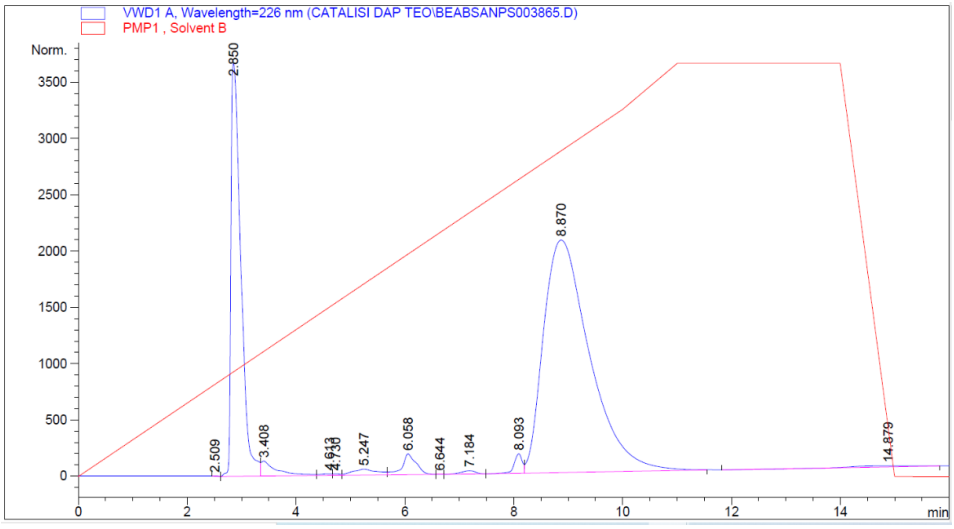

Figure 36 *Chromatogram of supernatant sample from BSA-Boc-Proline reaction.*

In the figure 36 this peak is only referred to pellet injection. Taking into account the previous chromatogram, it is easy to hypothesize that that t_R = 8.039 is proline peak, that in the Fig. 35 is 7.935

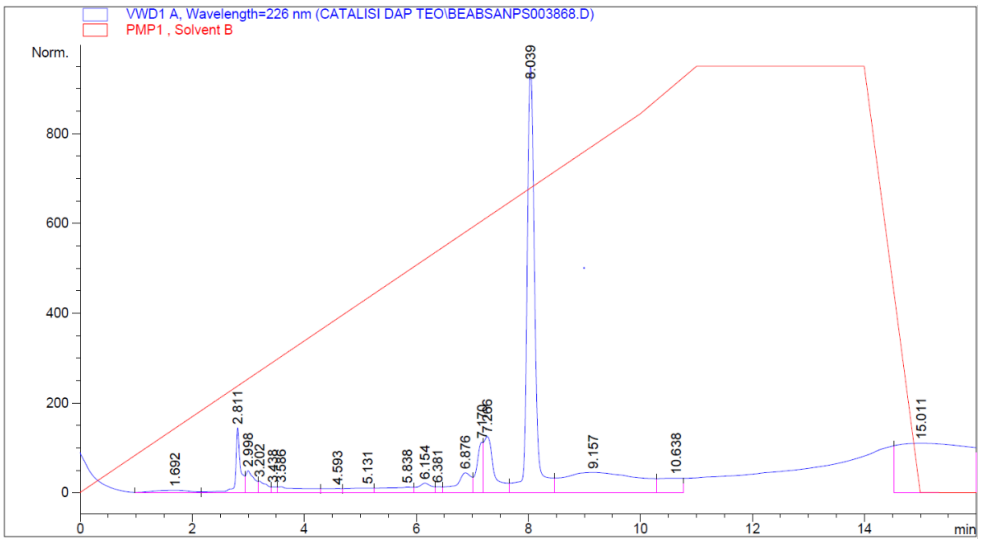

Figure 37 *Pellet chromatogram recovered after centrifugation of the solution.*

From these results we have decided to exclude the pellet, because we have understood that was only Proline which hasn't coupled with the protein.

Instead, supernatant is storage and incubated again with another aliquot of Boc-L-proline N-hydroxysuccinimide ester, to see how reaction proceeds. The first peak at 2.863 min is always N-hydroxysuccinimide; this time the second peak at 9.353 min is the same peak of figure 36, but with a shift. It means that our protein has been further functionalized, and that after centrifugation the product is in the aqueous phase. NHS presence can be removed by simply dialysis.

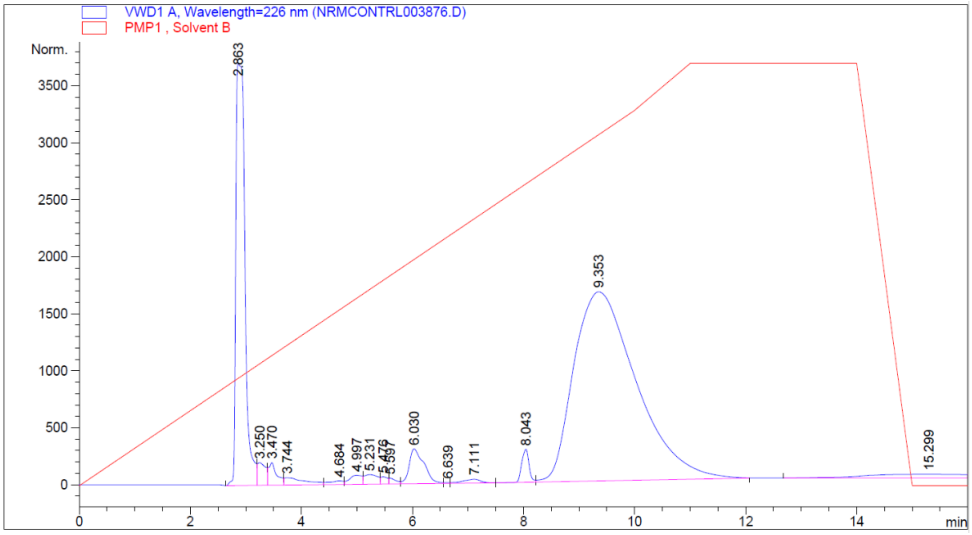

Figure 38 *Chromatogram of the product after the second addition of BOC-Pro-OSu.*

Boc removal after coupling step is generally made with TFA and DCM in ratio 1:1.[37] In this case we have seen by mass characterization that after Boc removal, BSA undergoes degradation. In figure 38 in the first spectra is possible to see the native BSA mass spectra, which gives as output a relative mass of 66,4 kDa, so in according with literature data. In the second image instead, there is the mass spectra of BSA functionalized with Proline after Boc deprotection. Looking at the peak is evident that they are distributed to low mass value, so it means that protein has been degraded.

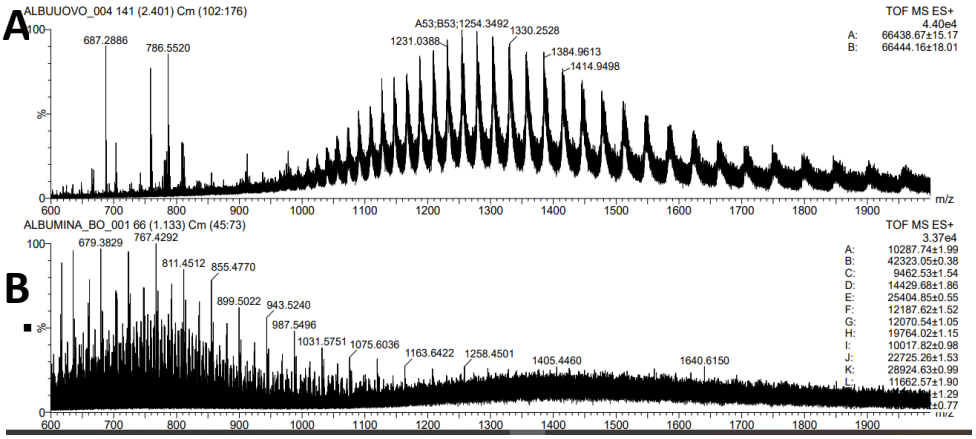

Figure 39 *Mass spectrometry spectra of native BSA (A) and BSA modified with Proline (B).*

This fact takes to the problem that in this way is difficult to quantify how much Proline has been coupled with every molecule of BSA. For this reason we have decided to proceed in another way.

3.5 BSA MODIFICATION WITH PROLINE NCA

The use of Proline N-carboxyanhydride (Proline NCA) is useful because it does not require protecting groups, and so avoid the use of solvents as TFA or DCM. NCA are highly reactive and they are used for peptides preparation by the ring-opening polymerization of a-amino acid N-carboxyanhydrides. Ring opening of NCA, during peptide chain formation, consists in the release of one molecule of carbon

dioxide and exposition of primary amine, which can react with the target molecule.[38]

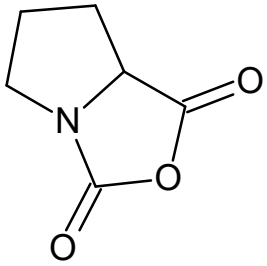

Figure 40 *Proline NCA chemical structure.*

Proline NCA is dissolved in acetonitrile and added to BSA solution at different time spot to follow reaction course through HPLC. This time we have used a C8 column and. The gradient is indicated in table 2:

Time (min)	%B
0	5
12	55
13	100
15	100
16	5

Table 2 *Gradient for BSA-ProNCA detection.*

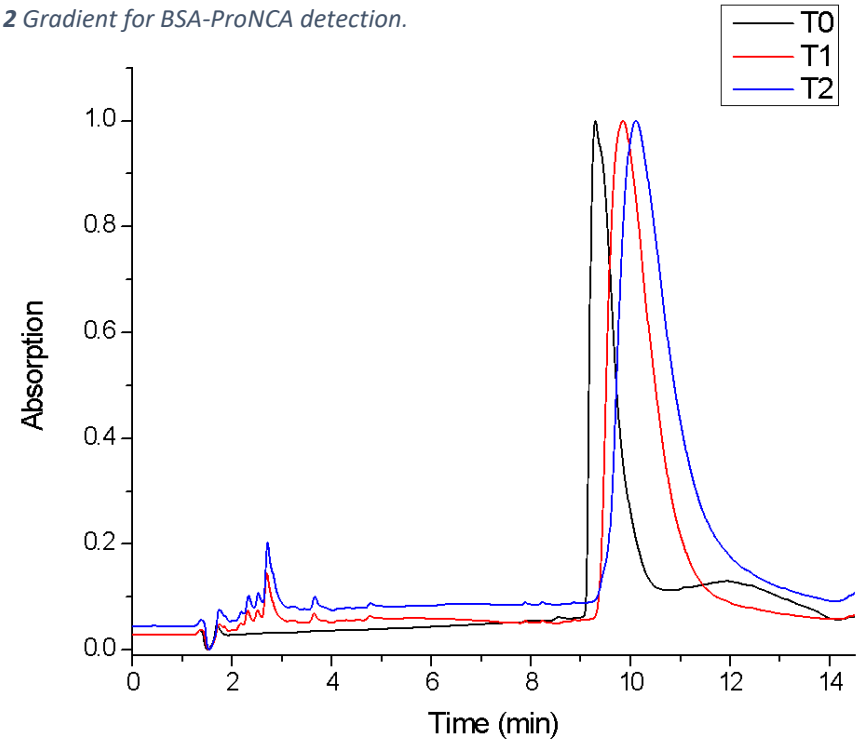

Figure 41 *Chromatogram and relative absorption spectra of BSA functionalization with Proline NCA. Black curve is relative only to native BSA. Red curve is reaction after the first addition of Proline NCA. Blue curve is after the second addition of Proline NCA.*

T0 → 9.294

T1 → 9.853

T2 → 10.131

The three retention time evidence the gradual functionalization of BSA during time. Every addition has been made every 20 minutes.

From mass characterization spectrum (Fig. 42B and 42C) is possible to see that protein has not been degraded. In the spectra B and C, peaks are related to BSA modification with Proline. In figure 42A instead there are the peaks relative to native BSA used as reference. It is evidence, the shift of modified BSA to high mas value. If we want to have an approximately idea of how many Proline has been coupled with the protein we can make same calculation. We can make an estimate looking at spectra C and charge distribution in spectra A. For example we can take the peak at 1.588,6649 and the relative charge, which is 42: we obtain a molecular weight of 68.312,5907. So, respect to BSA there is a mass shift of 1.912,59 Da. If Proline has a MW of 115,13 g/mol it means that this molecule has been functionalized with about 16 Proline molecules. Instead, if we take the peak at 1.875,0302 and its relative charge, 36, we obtain a MW of 6.7501,0872. In this case about 9 Proline residues have been coupled. Thus, by mass spectrometry measures it is possible to assume that BSA has been modified with Proline in a range between 10-20 molecules of Proline for each protein molecule.

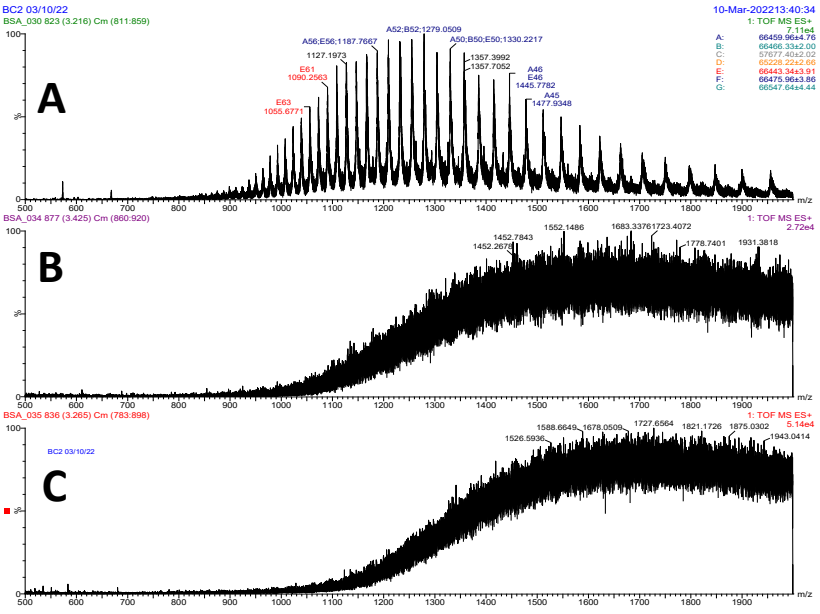

Figure 42 Mass spectrometry spectra

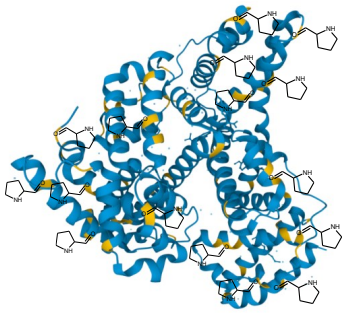

Figure 43 Graphical representation of BSA secondary structure functionalized with Proline. In yellow is possible to see Lysine residues.

3.6 BSA-PRO PROTEIN CORONA FORMATION.

The scaffold for our system formation can be used to create a protein corona around gold nanoparticles. As described in the introduction, we have made different addition of BSA. The characterization has been made on GNPs that have been growth, so that with an average diameter of 51.42 nm. Through TEM images we have tried to show the difference between the soft corona and hard corona.

In the first sample soft corona has been obtained incubating GNPs with modified BSA with Proline.

The first TEM image(Fig. 44) has been collected after the first addition of BSA-Pro. It is possible to appreciate thanks to staining protocol a thick shell around nanoparticle

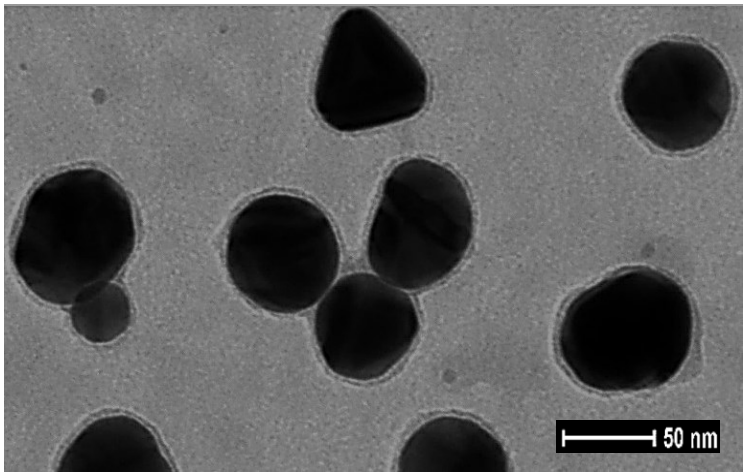

Figure 44 TEM image of growth GNPs with soft protein corona.

In Fig. n. 45 instead, there is the same sample, but in this case during sample preparation BSA-Pro solution has been added one more time, so here there is the double protein presence in solution.

It is not difficult to see the protein shell which cover NP. Thus in the second image is possible to see what is generally called “hard corona”.

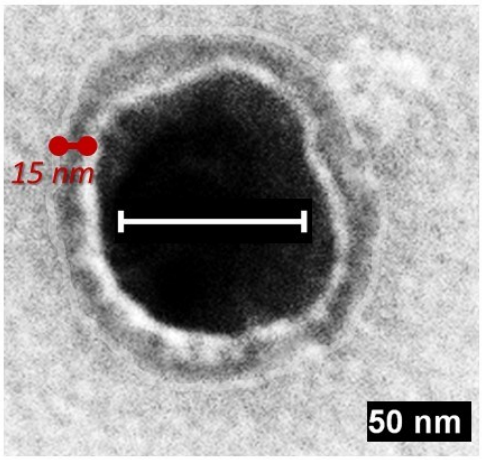

Figure 45 *TEM image of growth GNPs with hard protein corona.*

In the graph in figure 46, the DLS measures help us to have a quantitative idea of system size. While naked nanoparticles have a diameter of 52 nm, the first sample average diameter is 64 nm and in the second one is about 86 nm. Thus the difference between naked nanoparticle and functionalized ones is about 34 nm. This value could be indicative to have a first estimate of how many BSA molecules has adsorbed on GNP surface.

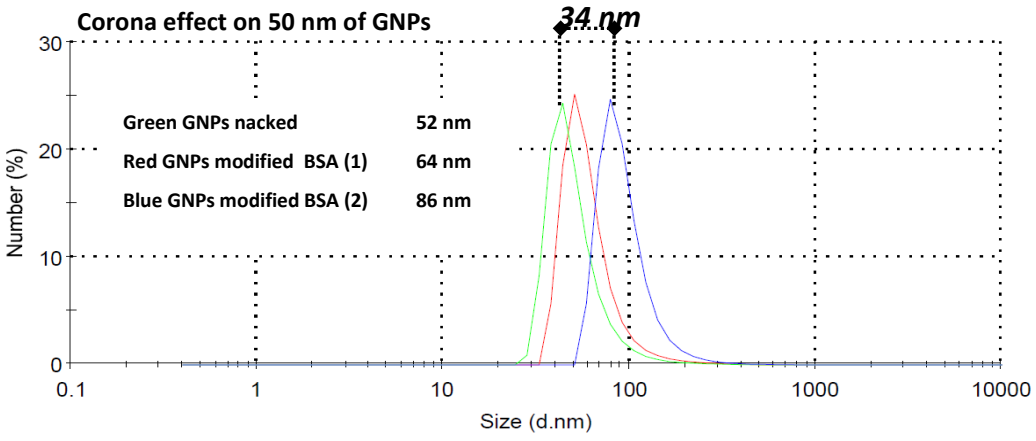

Figure 46 *DLS measures on GNPs modified with BSA.*

But from an analytical point of view is not sufficient. In fact is necessary to take into account that in that shell, various BSA molecules stands together, and not only are involved in the adsorption on gold surface, but also have contact with each other. Looking at BSA structure (Figure 47), we have measured three distances thinking about the maximum distance between some residues. In the three measures, the highest distance value is about 8 nm. This is not sufficient to calculate how many BSA molecules stay in that layer volume.

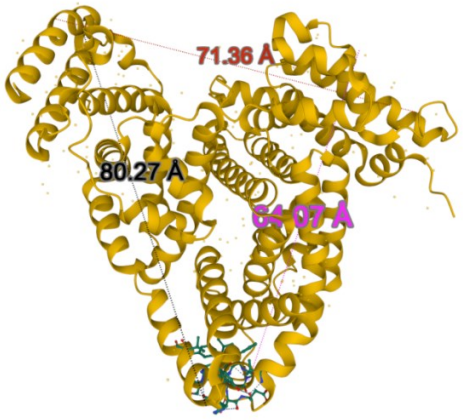

Figure 47

In fact, protein corona formation is a phenomenon that has to deal with complex kinetics parameters and equilibrium properties. According to the law of mass action, the partitioning between the various species (Free NPs- Protein saturated NPs- free proteins-protein bound to NPs) is described by K_D, the dissociation equilibrium coefficient.

$$k_D = \frac{c(NP)c^nP}{c(P_nNP)} = \frac{k_{off}}{k_{on}}$$

c(P_nNP): Protein saturated nanoparticles concentration;

c(NP) : Protein bound to nanoparticles concentration.

As reported in literature is difficult to have a complete characterization of protein corona, first for the difficult in NPs concentration determination. It would be necessary to use other techniques, as fluorescence correlation spectroscopy (FCS) and photothermal absorption correlation spectroscopy. Even if we do not have a precise quantification of protein corona, at the beginning of our experiments we have used chromatography, in the specific, Size exclusion chromatography (SEC).[7]

In SEC chromatography molecules are separated based on their size, through a filtration with a gel. [39] Gel is usually made of spherical beads containing pores with specific size distribution. Small molecules diffuse into beads and their flow and detection is retarded. On the contrary large molecules elute first, because they do not enter the pores. So, molecules are eluted in order of decreasing molecular weight. Eluent is composed by water and phosphate buffer (PBS). In the chromatogram in figure 48, is possible to observe the different retention time relative to a sample of GNPs-(BSA-Pro). By previous analysis we have seen that native BSA is detected after 12.085 minutes. The three distribution instead, are related to GNPs covered with BSA-Pro. Naked gold nanoparticles cannot be eluted in this type of column because citrate layer binds covalently to the matrix, which is composed by polysaccharides.

By peaks retention time, is evident that there is a certain size distribution, according to TEM images and also DLS measures.

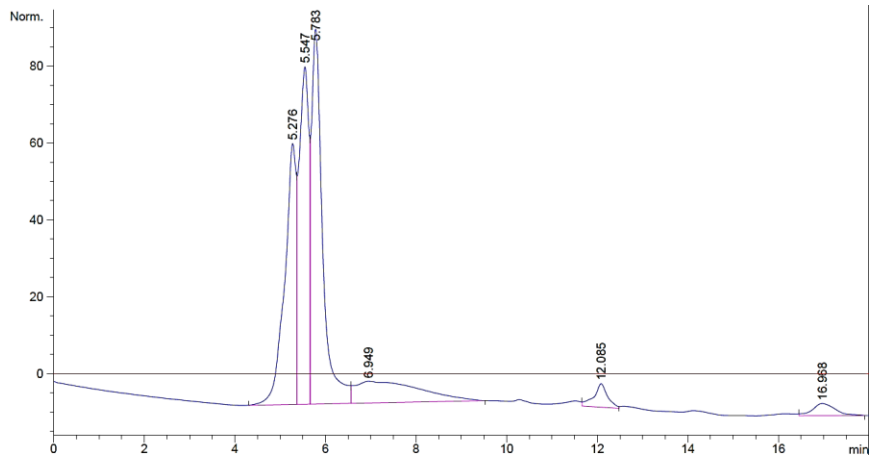

Figure 48 *Chromatogram relative to GNPs-(BSA-Pro) sample.*

3.7 CIRCULAR DICHROISM ANALYSIS ON BSA MODIFIED WITH PROLINE.

Circular Dichroism spectroscopy let to analyze chirality in biomolecules through their optical activity. The output is a spectrum given by the difference in the absorption of left and right circularly polarized light. It is used to study protein folding.

There are two absorption bands that make up the far-UV CD spectrum: a strong transition $\pi \rightarrow \pi^*$ at 190 nm and a weaker and broader $n \rightarrow \pi^*$ transition in the range of 210-220 nm. [40]

For the native BSA the two negative peak at 210 and 22 nm are characteristic of α-helical structure of protein. The typical spectrum for BSA, is the black one indicated in the graph below.

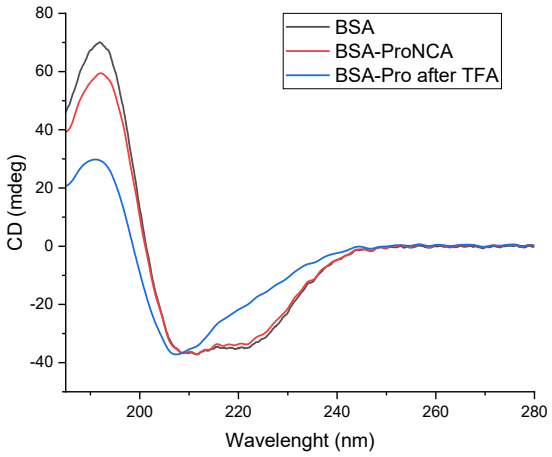

Figure 49 CD spectra .

The shape of the spectra gives us the idea of the difference between the three samples. By the CD spectra in figure 48 we can observe that BSA and BSA modified with Proline NCA curves are approximately overlapped, instead The BSA-Proline treated with TFA for Boc-removal is very different. To evaluate helix typology it is possible to use R parameter, which indicates the ratio of molar ellipticity between the two maximum negative.

When R=1 the structure is an α-helix and when R>1 indicates aggregates presence. Based on the calculated R value for the three samples we can say that in the first case, protein even if is modified, it keeps is natural structure. On the contrary the second sample has an R value smaller than the other two. So in this case protein has lost is native folding, probably due to degradation and formation of small peptide.

Sample	**θ_{208}**	**θ_{222}**	**R= $\theta_{222}/\theta_{208}$**
BSA	-36.35	-34.97	0.96
BSA-ProNCA	-36.07	-33.55	0.93
BSA-Pro (TFA)	-37.11	-20.98	0.56

Table 3 *Values of ellipticity and relative ratio for each sample.*

Circular Dichroism analysis on GNPs covered with BSA-Pro

Same analysis were made on GNPs incubated with native BSA and with BSA modified with Proline NCA. Wavelength range has been set between 180 and 280 nm to have the curves referred only to protein adsorption.

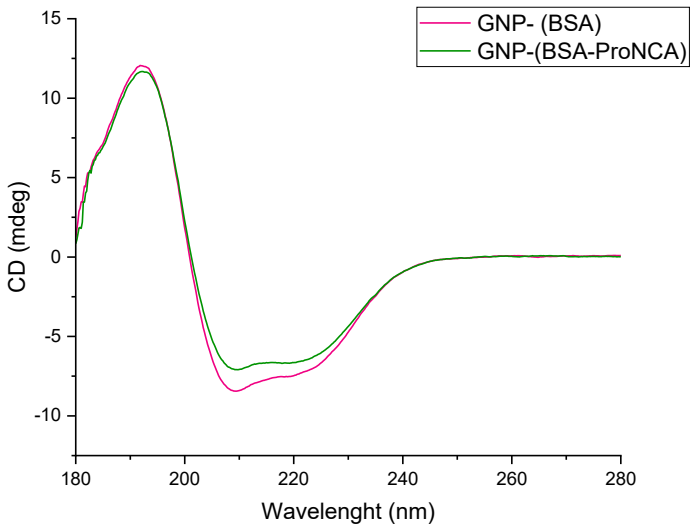

Figure 50 *CD spectra.*

Sample	**θ_{208}**	**θ_{222}**	**R= $\theta_{222}/\theta_{208}$**
GNP-BSA	-8.40	-7.50	0.90
GNP-(BSA-Pro)	-7.08	-6.66	0.94

Table 4 *Values of ellipticity and relative ratio for each sample.*

3.8 BSA LABELLING WITH FITC

BSA conjugation with FITC is useful to see nanogels one they are formed thanks to confocal microscopy. FITC is a common fluorophore used to label molecule. Every fluorophore has a chromogenic property and various reactive groups that can couple to specific functional groups of the target molecule. In this case the conjugation is a simple mechanism. The isothiocyanate group binds fluorescein to the amino and sulfhydric groups present in the protein. FITC fluorescence is due to its three-ring planar structure. It has a maximum absorption at 495 nm, while fluorescence emission is about 521 nm. Isothiocyanates are reactive toward nucleophilic group such as amines, sulfhydryls, and the phenolate ion of tyrosine side chains. However, FITC is highly selective for N-terminal amines in proteins because it is able to form stable products only with primary amine groups. The reaction proceeds with the attack of the nucleophile to the electrophilic carbon of the isothiocyanate group. Then, a thiourea bond is formed between FITC and the protein without leaving groups. [41]

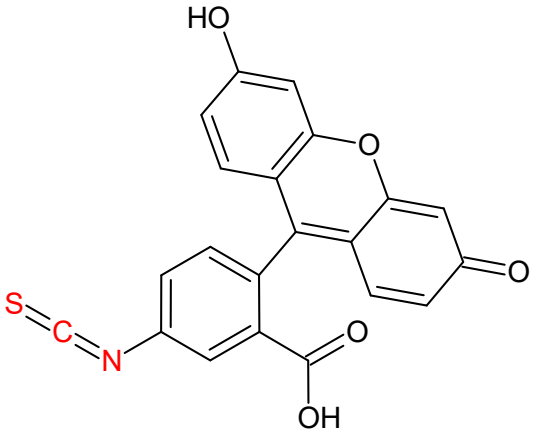

Figure 51 *FITC chemical structure.*

Also in this case the real functionalization with FITC has been followed thanks to HPLC analysis. In this case we have used a C4 column and gradient is in table 5 :

Time (min)	% B
0	5
8	50
9	100
12	100
13	5

Table 5 *Gradient.*

In the first chromatogram (Fig. 52) there is only BSA injection, that is detected after 9.784 minutes. This is the first reference.

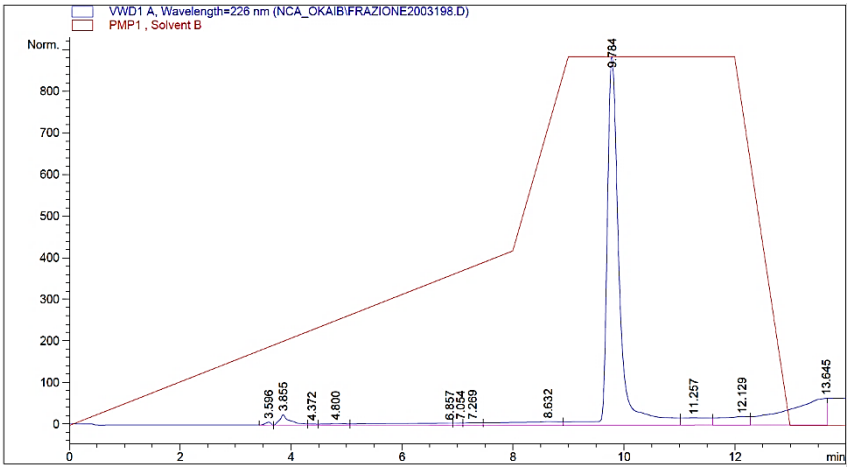

Figure 52 *Native BSA chromatogram.*

The second reference instead is the peak relative to FITC (Fig.53). In this case is necessary to change lamp wavelength for its detection, to 521 nm. FITC Tr is 12.339 minutes.

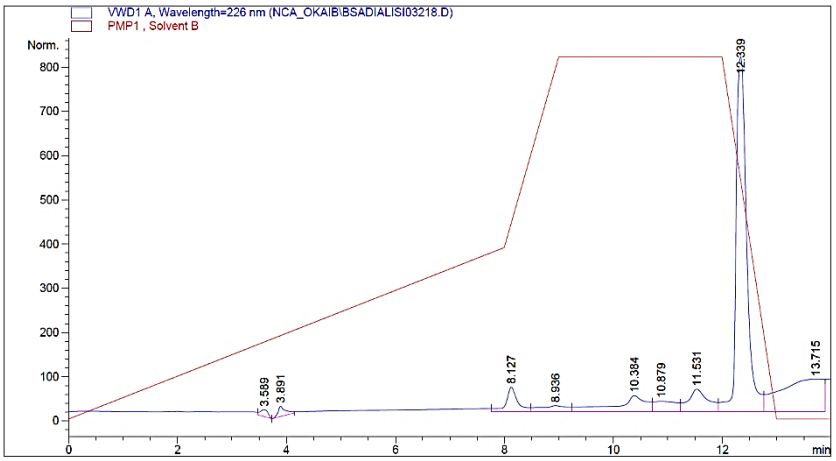

Figure 53 *FITC chromatogram.*

FITC addition and BSA labelling is gradually followed. After incubation BSA peak has a shift and t_R increases gradually. In this chromatogram we can say that the second peak is FITC, thanks to the reference injection made before; the first peak at 10.196 minutes is BSA that is gradually functionalized with FITC.

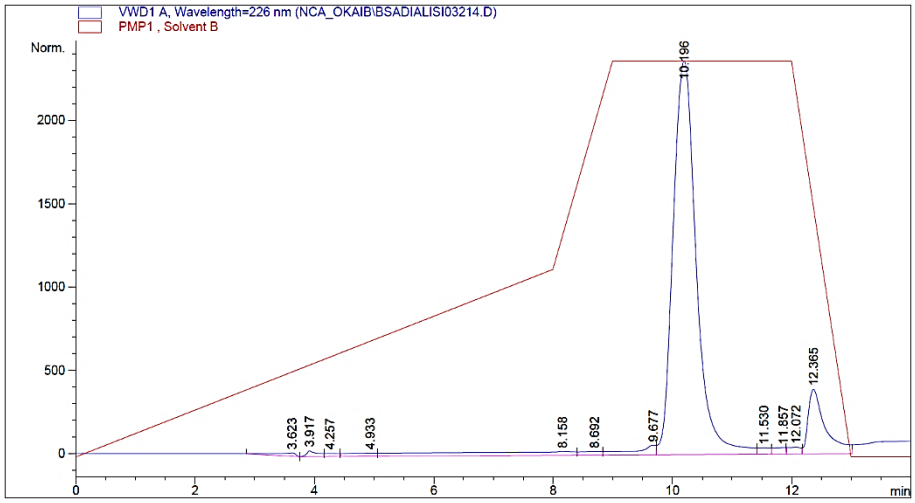

Figure 54 *BSA-FITC chromatogram after 30 minutes.*

After 1 hour of incubation we have made another injection that has revealed that FITC was continuing to label the protein. In fact the first peak has just shifts again and is detected after 10.473 minutes.

At this point the reaction is stopped, because in this case FITC is just a tool to have a direct visualization of our systems, one time that they are synthetized.

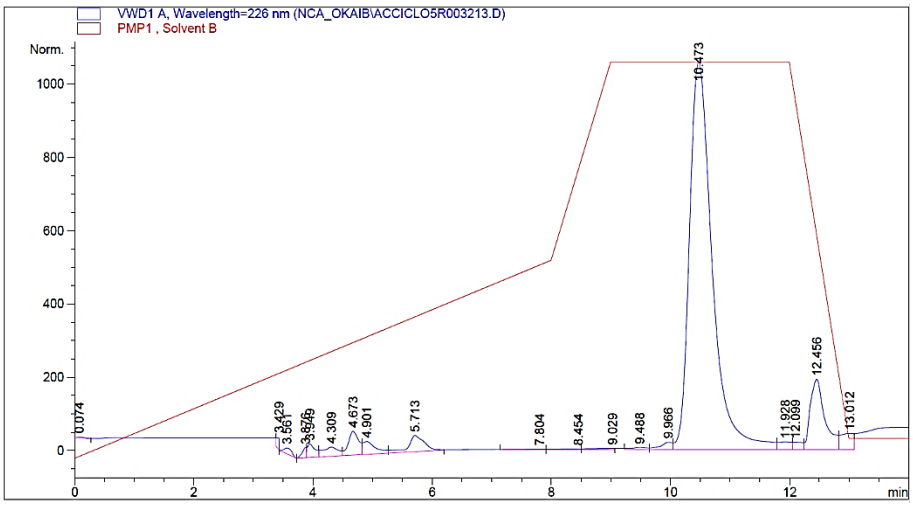

Figure 55 *BSA-FITC chromatogram after 1 hour of incubation.*

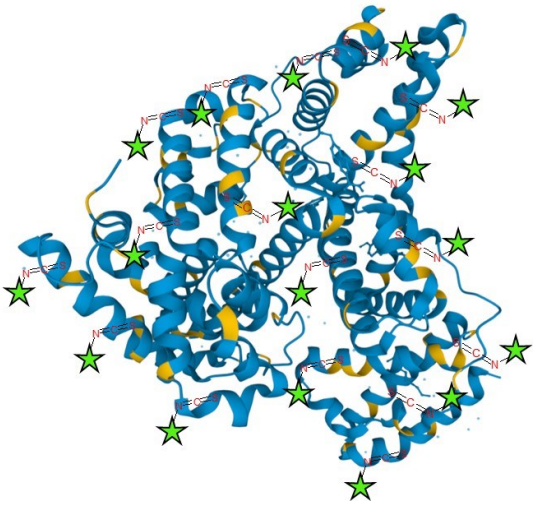

Figure 56 BSA structure after labeling with FITC.

3.9 POLYMERIZATION PROCESS.

At this point our system is composed by a gold nanoparticle with a hard protein corona composed by BSA protein functionalized with Proline amino acid and labelled with a fluorophore for the direct visualization.

Polymerization is our second step synthesis. For this aim BSA has to be further functionalized, because polymerization needs different elements:

- Radical for polymerization starting point → Vinyl termination;
- Crosslinker → *N,N′*-Methylenebisacrylamide;
- Monomer → N-Isopropylacrylamide / 4-vinylpyridine;
- Iniziator → 2,2′-azobis(2-methylpropionamidene) dihydrochloride.

3.9.1 BSA functionalization with Butanoic acid.

Butanoic acid is used to give to BSA vinyl termination, for the polymerization beginning. So the metallic core acts as seed for the process. The presence of carboxylic group is used to bond this molecule to amine group of BSA residues. In

this way we obtain a protein with a lot of vinyl termination. When butanoic acid is incubated with protein, it becomes more hydrophobic.

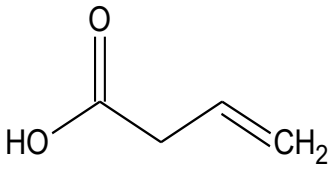

Figure 57 3-butanoic acid chemical structure.

Its contribution to polymerization has revealed essential. In fact, when we have tried to have a polymerization of NIPAM with initiator and crosslinker, but without the vinyl function on BSA, nanoparticles solution collapse and precipitate. This happens because, without a "starting point", polymerization start casually, so the hydrogels has not a "guide". The result is an uneven polymerization, that can catch nanoparticles, make them unstable. [42]

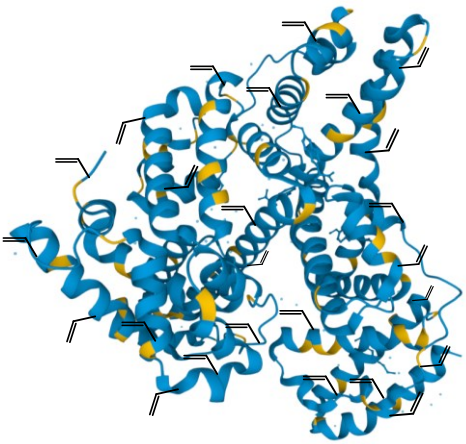

Figure 58 BSA structure with vinyl termination after modification with butenoic acid.

3.9.2 Polymerization p-NIPAM

Polymerization occurs through a classical free radical polymerization activated by heat, in fact reaction is made at 70°C. [43]

We have opted to use NIPAM as monomer for hydrogels formation, based on the work of Contreras-Caceres and his colleagues. In the first part of their experiments they prepare hydrogels with 4VP using as template gold nanoparticles. Looking at

TEM images present in their work it is evident that polymerization does not happen homogeneously around NP. In fact NP remains in a peripherical localization. They have described these structures with a “Janus” morphology. [18]

For this reason, we have synthetized p-NIPAM hydrogels, because in this case there is a homogeneous polymerization around the spherical nanoparticle.

TEM images below show the complete system. At the center is possible to see GNP.

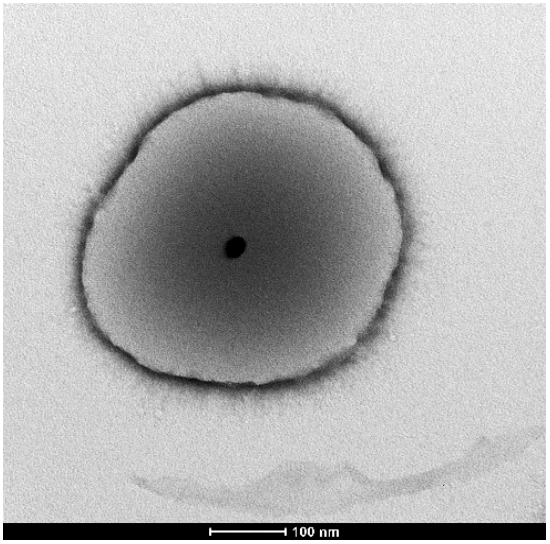

Figure 59 *TEM image after polymerization around GNPs.*

Despite the centrifugation purification step could force the aggregation of these nanogels. From figure 60 it is clear that after the redispersion of the pellet, nanogels are not aggregated.

Looking at our aim, for catalytic process, this is an interesting aspect about the re-use of these nanogels. For example, after the catalytic reaction is finished, it could be easy to separate products from catalysts, simply by centrifugation. The pellet contains aggregated nanogels, that can be separated just dissolved then in an appropriate water volume.

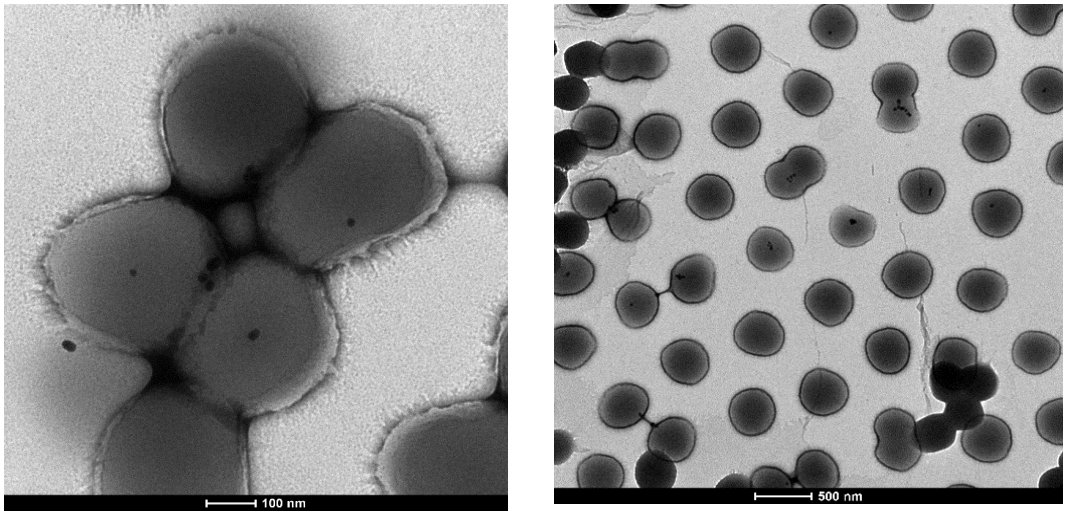

Figure 60 TEM images.

Thanks to DLS it is possible to estimate the hydrodynamic size (volume distribution) of these hybrid nanosystems. The two peaks visible in the graph below evidence the presence of two distribution, that indicate also a small population of aggregate nanogels. But looking at peak height is normal to take into account only the first one.

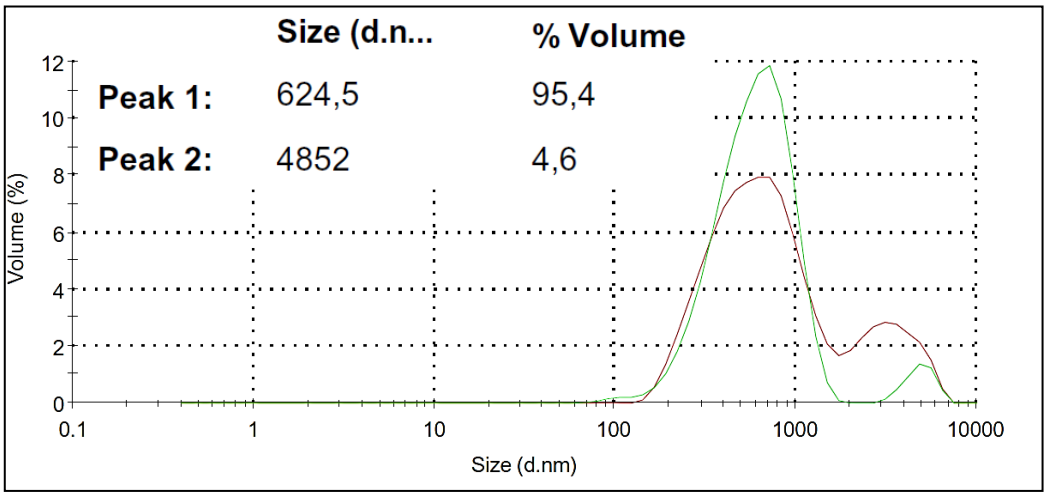

Figure 61 DLS spectra.

3.10 ETCHING

The final step, is gold core oxidation to remove nanoparticle and obtain an hollow structure with a catalytic cavity.

GNP remotion is obtained through oxidation using CTAB and $HAuCl_4$.The chemical reaction is schematized below [44]. The dissolution of GNPs goes following this reaction:

$$AuCl_4^- + 2Au^0 + 2Cl^- = 3AuCl_2$$

In Liz-Marza et al. Work, they underline the fact that AuCl4- ions are bound to CTAB micelles. CTAB plays a fundamental role in GNPs oxidation mechanism. CTAB concentration has to be over critical micelle concentration (c.m.c)[45]; in this way CTAB acts as a carrier for $HAuCl_4$ ions, let a gradual oxidation of GNPs. The main advantage of this type of process is that it does not annoy all the other elements of the system, not modified BSA and neither the polymer.

The first characterization has been made with TEM. In figure 62 is possible to see the hole at the center of the system with the polymeric shell around.

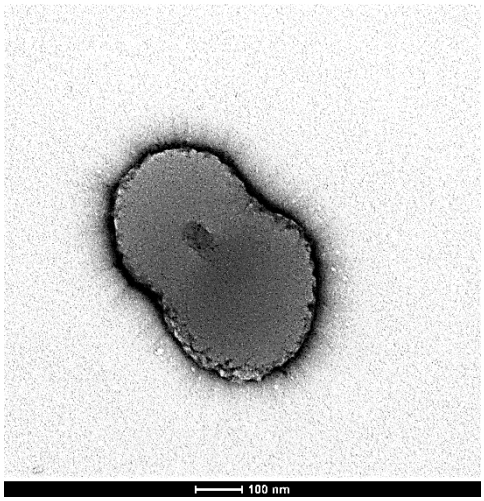

Figure 62 *TEM image after etching process.*

In the TEM images below (Fig. 63) it is possible to appreciate two systems. In one of these GNP has been oxidated, while in the nearby one the nanoparticle is still

inside the hydrogel. Also in this case is necessary to adjust CTAB/ $HAuCl_4$ concentration to have an homogeneous oxidation.

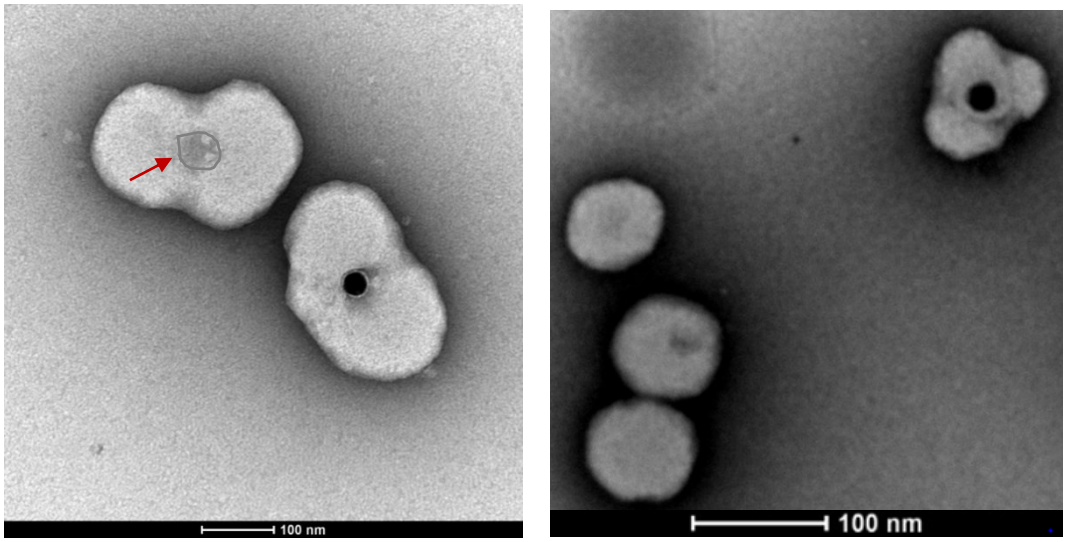

Figure 63 TEM images.

Gold core oxidation is also visible at UV-spectrum (Fig. 64), where is evident the absence of the typical absorbance peak at 520 nm of GNPs.

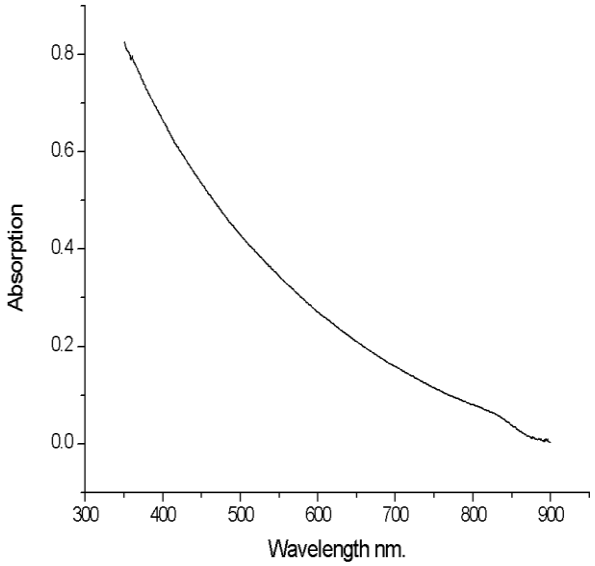

Figure 64 UV-spectrum.

Thanks to a solid state fluorimeter (Dr. Gregorio Bottaro, CNR UNIPD) we detected the emission fluoresce of nanogels. In the spectrum in figure 65, the emission peak is about a 523 nm, in fact FITC emission is around this value.

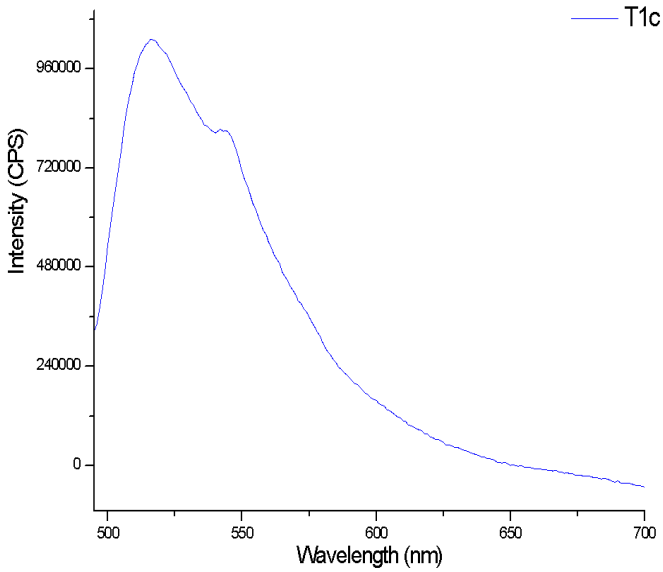

Figure 65 *Fluorescence emission spectrum.*

A further characterization has been made with confocal microscopy (Dr.ssa Ilaria Fortunati, DiSC, UNIPD, that let us to see the hollow nanogels dispersion thanks to the detection of the fluorescence emission of FITC used to label BSA (Fig. 66). In confocal microscopy illuminating light passed through the sample as uniformly as possible over, The theory of confocal microscopy is that the illumination optic is focused on the same diffraction-limited spot, which is moved on the sample to build the complete image on the detector. [46]

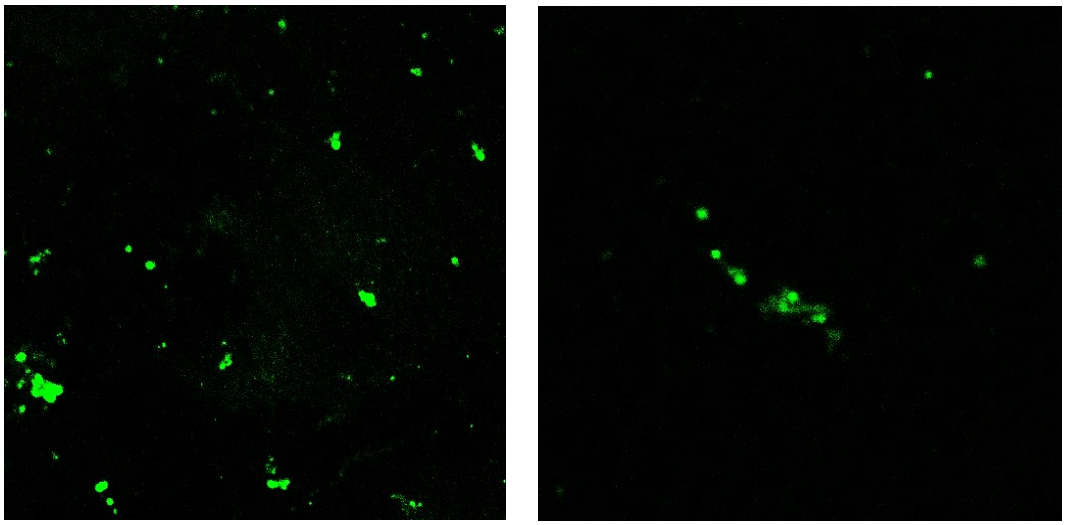

Figure 66 *Confocal microscopy images.*

3.11 CATALYSIS REACTION

Aldol reaction is a reaction which involves a molecule with an aldehydic function and a ketonic molecule. They are the most important carbon-carbon bond forming reactions. The disadvantages about Proline[47] use as catalyst is that for aldol reactions a large amount is necessary and there is no proof in literature for a way to recycle them and separated them from products.

As described in the introduction chapter Proline could acts as catalyst Proline is a chiral molecule, inexpensive and available in both enantiomeric forms. In the way to reproduce these results we have follow a previous work in literature. [48]

Our results by using nitrobenzaldheyde and cyclohexanone is reported in figure 68. We found that by using 10% catalyst (L-Pro) we obtain a rapid conversion (8 hr) in quantitative yield of the anti addition product in the (r,s) configuration enantiomer. Thus by using the modified BSA-L-Pro catalyst, in similar experimental condition we found a quantitative conversion in 24 hr, with the formation of the syn addition product in the (r,s) configuration enantiomer.

As references 1H NMR spectra we report the two Syn and Anti products (Fig. 67). The products obtained by the aldolic reaction, independently, from which catalyst has been used, have been characterized with NMR spectroscopy. The two enantiomeric forms have been separated with flash chromatography. For NMR characterization, product has been dissolved in chloroform ($CDCl_3$). The obtained spectra has confirmed the two products formation. We have confront this spectra and their relatives peaks with data find in literature. [49]

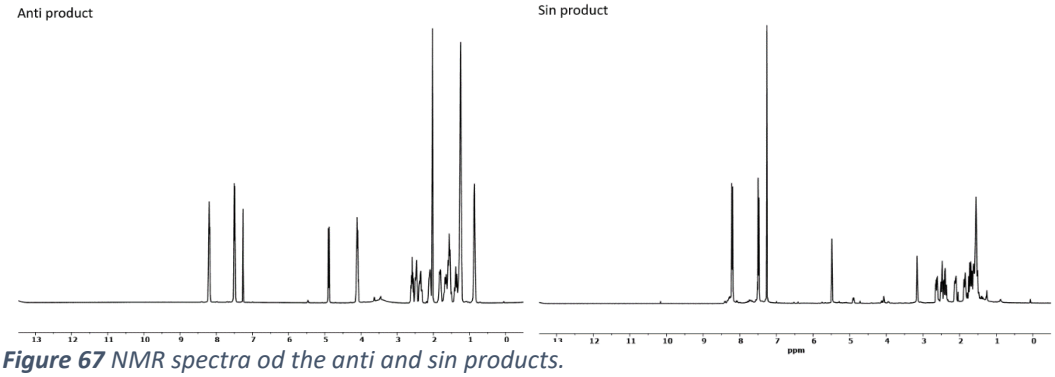

Figure 67 *NMR spectra od the anti and sin products.*

We run an additional catalytic experiment by using BSA-**L/D**-Pro in the way to control the effect of the chirality on the modified protein. In this case, we found a lower conversion together with the formation of an almost equimolar amount of both, the syn and anti product generated in this non selective reaction. Looking at the chromatogram in fig. 67 C, we observe three peaks. The first one is the substrate. The other two peaks are relative to the two diastereomers. In the other chromatograms, peak product is just one, because the two enantiomeric forms cannot be differentiated by HPLC. This results are very promising, because the modified protein seem to work in a similar manner of L-proline.

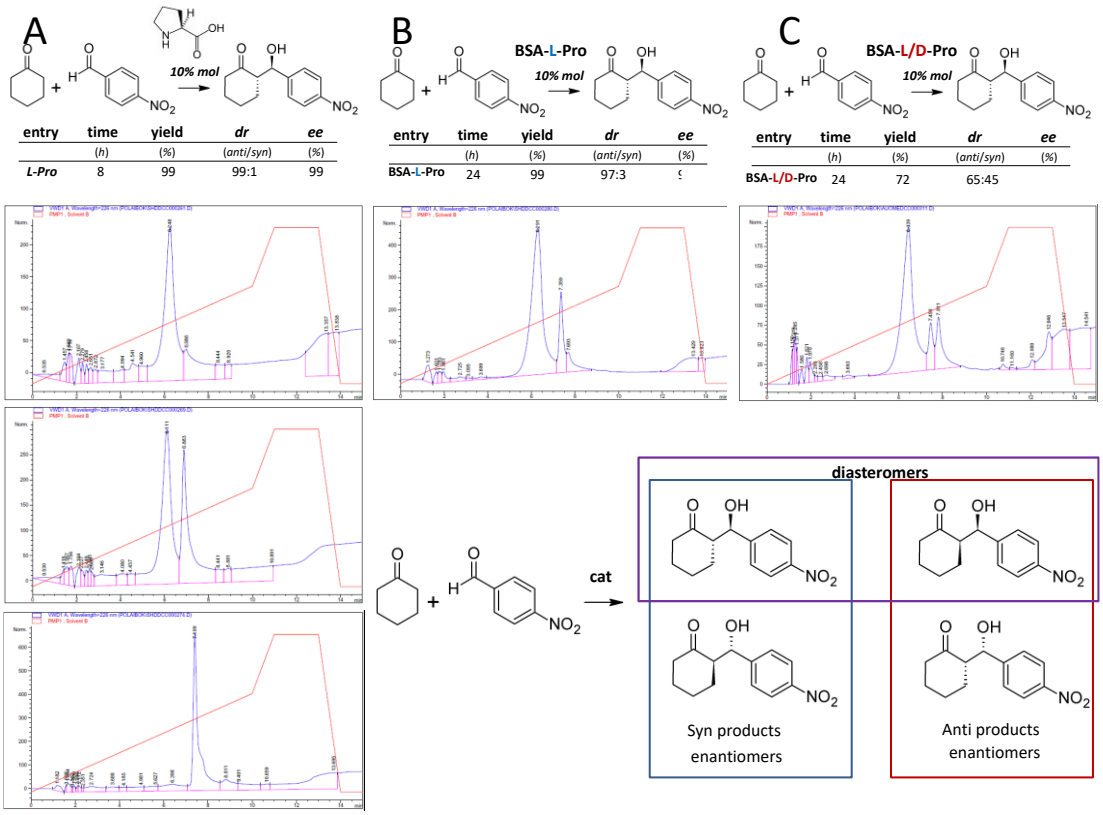

Figure 68 *Aldolic reaction between nitrobenzaldehyde and cyclohexanone catalyzed by:* ***A)*** *L-Proline;* ***B)*** *BSA-L-Proline;* ***C)*** *BSA-L/D-Proline.*

In the next step, we decide to reproduce literature results, where a small proline based dipeptide is linked to a gold nanoparticle. In work they shown aldol reaction between two substrate in PEG 400 medium. NH-Pro-Cys-OH was synthetized by

solid-phase synthesis as described in paragraph 2.11 and anchored to GNp following the reported protocol. As carbonyl compound we have used nitrobenzaldehyde, while as ketone, cyclohexanone. We used this peptide-GNPs systems as control to compare the catalytic performance on our BSA-L-Pro-GNPs systems.

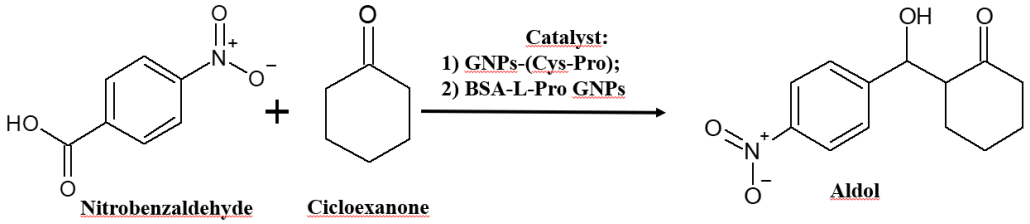

Figure 69

In the first experiment that we will call "control" we have based on that find in literature, so we have synthetie GNPs functionalized with Cysteine-Proline dipeptide. Control experiment takes place in PEG-400 as solvent. We have followed reactions through HPLC analysis, using a C8 column with the following gradient (Table. 6):

Time (min)	%B
0	10
10	90
11	100
12	100
13	10

Table 6 *Gradient.*

We follow the reaction by HPLC. In fig. 70 the first chromatogram is referred to nitrobenzaldehyde, which has a t_R of 6.900 minutes. Next we added the GNP-Cys-Pro catalyst. After 12 hours we recorded the second chromatogram (Fig. 69). We found the formation of the aldol product. After 24 hours the reaction completely converted the nitrobenzaldhyde into the aldol product.

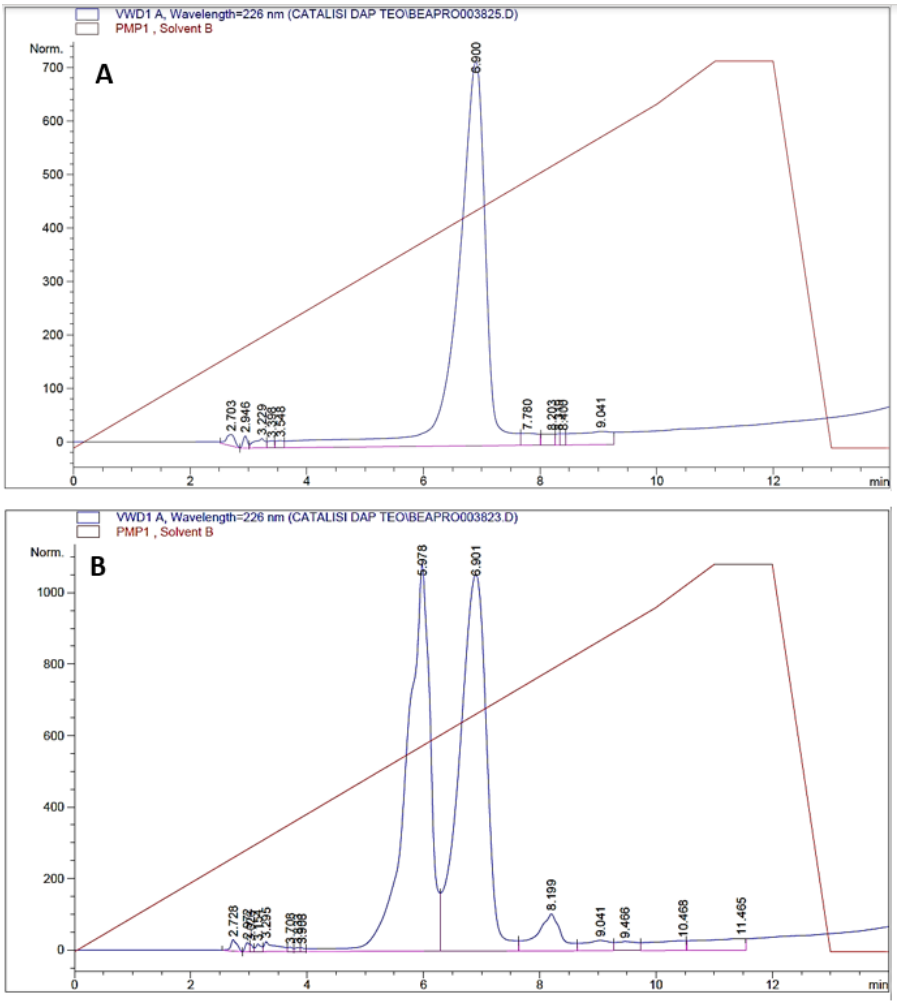

Figure 70 *(A) Nitrobenzaldhyde chromatogram. (B) Reaction chromatogram after catalyst addition.*

In the second experiment we have made the same steps, both in preparation both in analysis, but this time catalyst is BSA-Pro GNPs and reaction is in aqueous medium. We have used C8 column with the same gradient of the control experiment. The first chromatogram (Fig. 71) is always referred to nitrobenzaldehyde which is detected after 7.061 minutes. After 12 hours the situation is described in the chromatogram B: the new peak at 6.154 minutes is the

product which is still forming, while the second one is substrate. The second injection has been made after 24 hours from the first and it is possible to observe that product amount has changed, about half part of the substrate has been converted in the product.

For the analysis of the reaction we have to change gradient, because with the previous one we could not distinguish well the product from the substrate.

Time (min)	%B
0	10
10	90
11	100
14	100
15	10

Table 7 Gradient.

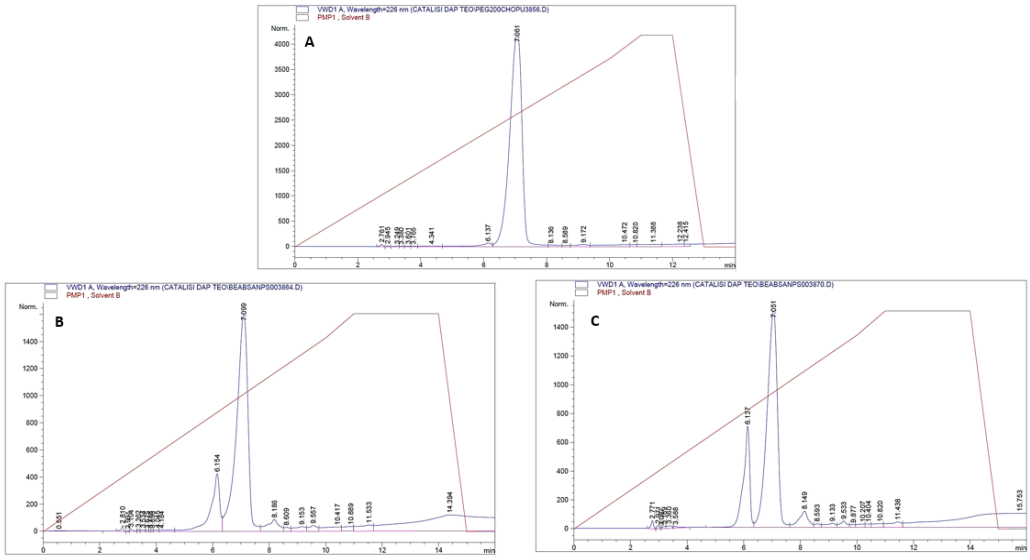

***Figure 71** (A) Nitrobenzaldhyde chromatogram; (B) reaction curse after 12 hours; (C) Conversion after 24 hours.*

Thus the control experiment help us to follow the reaction catalyzed by BSA-L-Pro GNPs. In this way we can have an idea of product formation. The product obtained by the last experiments, so catalyzed by BSA-Pro-GNPs are identically to those obtain from Pro catalyzed reaction.

Thus, we have demonstrated how GNPs decorated with a common modified protein, as BSA, may have a catalytic activity toward aldol condensation similar to

that of L-Proline. We are currently exploring the performance of the hollow nanogels enclosing the functional protein.

4 CONCLUSIONS

Following the aim of our Project we were able to combine three different nanomaterials to create a new one able to perform catalytic activity toward a C-C bond formation.

In the way to mimic proline as catalyst toward a stereoselective aldol condensation we added chemically Proline to the Lys amine on BSA protein. The novel protein displayed similar stereoselective capability than the original proline. We may assume that the adjacent Asp and Glu residues along the primary sequence of BSA give the required assistance of the carboxylic unit to the secondary amine of the proline, as occurring in the case of the single amino acid (Pro).

Moreover this protein was used as corona ligand to the surface of gold nanoparticle. The resulting hybrid system was fully characterized and successfully applied to the same aldolic condensation reaction.

In the way to create an hallow nanogels, composed by an empty inner cavity fully-cover by the catalytic protein, we used the corona nanoparticle as template to, in micelle, polymerize acrylamide derivatives. We follow a reported protocol for the polymerization and we obtained the core/shell/shell metallic/proteic/nanogel systems.

By removing the metallic nanoparticle core, via selective etching, we obtained the hollow nanogel with the imprinted protein in its inner cavity.

We are currently exploring the catalytic properties of this novel nanosystem.

5 FUTURE PERSPECTIVES

During this work of thesis we have synthetized three-dimensional systems composed by a hydrogel and a modified protein with catalytic activity for aldolic reactions. One of the main limit is that it could be better to have a standard procedure to have less size distribution during polymerization process. In fact we have seen that a lot of the formed systems have a diameter above nanometric level. NIPAM hydrogels are used in tissue engineering, for drug delivery, as polymeric support for cell growth, because it is a biocompatible molecule.

Looking at the system that we have synthetized they could be applied in different fields. For example, they could be used at industrial level. Aldolic condensation are applied in pharmaceutical and cosmetic industry, too.[50] Thinking about NIPAM characteristics, its sensibility to temperature can be exploited in industrial process for product release, and then catalysts recovery.

Thinking about drug delivery system, our nanogels could be useful to catalyze aldolic reactions inside cells. In fact a lot of aldolic reactions are involved in cellular metabolic pathways. For example in Kreb's cycle there is the addition of oxaloacetate to acetyl CoA, or in gluconeogenesis, where glyceraldehyde-3-phosphate (GAP) and dihydroxyacetone phosphate (DHAP) condense together to form fructose 1,6-bisphosphate.[51] Normally these reactions are catalyzed by enzymes. In some cases, it could happen that enzymes do not work well or in other cases person could be deficient for that specific enzyme; all this could be the origin of different disease of cause of inflammation. In these cases our systems may act as catalysts to overcome natural enzyme lack. Obviously it is necessary to investigate how these systems interact with cells, how can be internalized and especially how they are degraded after the reaction.

These are only some hypothesis, but the system could be modified for other applications, just simply modifying BSA with other amino acids. For example with a three-peptide known to have a catalytic activity, as the triad Serine, Histidine, Asparagine. In this case is necessary to make also docking studies to understand if peptides can interact not only with other BSA residues, but also between each other.

In our case, we have just modified BSA with one amino acid, so there is less risk of unwanted interactions.

In this chapter we have nominated just few applications, but organo-catalysis has a big variety of shades and a lot of works are in progress to improve this field.

6 BIBLIOGRAPHY

(1) Mohammed, I. A.; Al-Gawhari, F. J. Gold Nanoparticle: Synthesis, Functionalization, Enhancement, Drug Delivery and Therapy: A Review. 2020, *11* (6), 23.

(2) Bolaños, K.; Kogan, M. J.; Araya, E. Capping Gold Nanoparticles with Albumin to Improve Their Biomedical Properties. *Int. J. Nanomedicine* 2019, *Volume 14*, 6387–6406. https://doi.org/10.2147/IJN.S210992.

(3) Kimling, J.; Maier, M.; Okenve, B.; Kotaidis, V.; Ballot, H.; Plech, A. Turkevich Method for Gold Nanoparticle Synthesis Revisited. *J. Phys. Chem. B* 2006, *110* (32), 15700–15707. https://doi.org/10.1021/jp061667w.

(4) Grys, D.-B.; de Nijs, B.; Salmon, A. R.; Huang, J.; Wang, W.; Chen, W.-H.; Scherman, O. A.; Baumberg, J. J. Citrate Coordination and Bridging of Gold Nanoparticles: The Role of Gold Adatoms in AuNP Aging. *ACS Nano* 2020, *14* (7), 8689–8696. https://doi.org/10.1021/acsnano.0c03050.

(5) Ogarev, V. A.; Rudoi, V. M.; Dement'eva, O. V. Gold Nanoparticles: Synthesis, Optical Properties, and Application. *Inorg. Mater. Appl. Res.* 2018, *9* (1), 134–140. https://doi.org/10.1134/S2075113318010197.

(6) Gaspar, R. Pushed off Target with Proteins. *Nat. Nanotechnol.* 2013, *8* (2), 79–80. https://doi.org/10.1038/nnano.2013.11.

(7) Pino, P. del; Pelaz, B.; Zhang, Q.; Maffre, P.; Nienhaus, G. U.; Parak, W. J. Protein Corona Formation around Nanoparticles – from the Past to the Future. *Mater Horiz* 2014, *1* (3), 301–313. https://doi.org/10.1039/C3MH00106G.

(8) Jahanban-Esfahlan, A.; Ostadrahimi, A.; Jahanban-Esfahlan, R.; Roufegarinejad, L.; Tabibiazar, M.; Amarowicz, R. Recent Developments in the Detection of Bovine Serum Albumin. *Int. J. Biol. Macromol.* 2019, *138*, 602–617. https://doi.org/10.1016/j.ijbiomac.2019.07.096.

(9) Vashist, A.; Kaushik, A.; Ghosal, A.; Nikkhah-Moshaie, R.; Vashist, A.; Dev Jayant, R.; Nair, M. Chapter 1. Journey of Hydrogels to Nanogels: A Decade After. In *Smart Materials Series*; Vashist, A., Kaushik, A. K., Ahmad, S., Nair, M., Eds.; Royal Society of Chemistry: Cambridge, 2017; pp 1–8. https://doi.org/10.1039/9781788010481-00001.

(10) Karg, M.; Pich, A.; Hellweg, T.; Hoare, T.; Lyon, L. A.; Crassous, J. J.; Suzuki, D.; Gumerov, R. A.; Schneider, S.; Potemkin, Igor. I.; Richtering, W. Nanogels and Microgels: From Model Colloids to Applications, Recent Developments, and Future Trends. *Langmuir* 2019, *35* (19), 6231–6255. https://doi.org/10.1021/acs.langmuir.8b04304.

(11) Zhang, X.; Malhotra, S.; Molina, M.; Haag, R. Micro- and Nanogels with Labile Crosslinks – from Synthesis to Biomedical Applications. *Chem. Soc. Rev.* 2015, *44* (7), 1948–1973. https://doi.org/10.1039/C4CS00341A.

(12) Suzuki, D.; Horigome, K.; Kureha, T.; Matsui, S.; Watanabe, T. Polymeric Hydrogel Microspheres: Design, Synthesis, Characterization, Assembly and Applications. *Polym. J.* 2017, *49* (10), 695–702. https://doi.org/10.1038/pj.2017.39.

(13) Corrigan, N.; Jung, K.; Moad, G.; Hawker, C. J.; Matyjaszewski, K.; Boyer, C. Reversible-Deactivation Radical Polymerization (Controlled/Living Radical Polymerization): From Discovery to Materials Design and Applications. *Prog. Polym. Sci.* 2020, *111*, 101311. https://doi.org/10.1016/j.progpolymsci.2020.101311.

(14) Moad, G.; Chiefari, J.; Mayadunne, R. T. A.; Moad, C. L.; Postma, A.; Rizzardo, E.; Thang, S. H. Initiating Free Radical Polymerization. *Macromol. Symp.* 2002, *182* (1), 65–80. https://doi.org/10.1002/1521-3900(200206)182:1<65::AID-MASY65>3.0.CO;2-E.

(15) Doña, M.; Ortega-Rodriguez, A.; Alarcón-Fernández, C.; López-Romero, J. M.; Contreras-Cáceres, R. Effect of the Cross-Linking Density on the Gold Core Oxidation in Hybrid Core@shell Au@pNIPAM and Janus Au@p4VP Systems. *Colloids Surf. Physicochem. Eng. Asp.* 2020, *584*, 124014. https://doi.org/10.1016/j.colsurfa.2019.124014.

(16) Li, S.; Zhu, M.; Whitcombe, M. J.; Piletsky, S. A.; Turner, A. P. F. Molecularly Imprinted Polymers for Enzyme-like Catalysis. In *Molecularly Imprinted Catalysts*; Elsevier, 2016; pp 1–17. https://doi.org/10.1016/B978-0-12-801301-4.00001-3.

(17) Clara-Rahola, J.; Moscoso, A.; Belén Ruiz-Muelle, A.; Laurenti, M.; Formanek, P.; Lopez-Romero, J. M.; Fernández, I.; Diaz, J. F.; Rubio-Retama, J.; Fery, A.; Contreras-Cáceres, R. Au@p4VP Core@shell PH-Sensitive

Nanocomposites Suitable for Drug Entrapment. *J. Colloid Interface Sci.* 2018, *514*, 704–714. https://doi.org/10.1016/j.jcis.2017.12.072.

(18) Clara-Rahola, J.; Moscoso, A.; Belén Ruiz-Muelle, A.; Laurenti, M.; Formanek, P.; Lopez-Romero, J. M.; Fernández, I.; Diaz, J. F.; Rubio-Retama, J.; Fery, A.; Contreras-Cáceres, R. Au@p4VP Core@shell PH-Sensitive Nanocomposites Suitable for Drug Entrapment. *J. Colloid Interface Sci.* 2018, *514*, 704–714. https://doi.org/10.1016/j.jcis.2017.12.072.

(19) Schneider, H. A. Flexibility and Phase Transitions of Polymers. *J. Appl. Polym. Sci.* 2003, *88* (6), 1590–1599. https://doi.org/10.1002/app.11834.

(20) Capella, V.; Rivero, R. E.; Liaudat, A. C.; Ibarra, L. E.; Roma, D. A.; Alustiza, F.; Mañas, F.; Barbero, C. A.; Bosch, P.; Rivarola, C. R.; Rodriguez, N. Cytotoxicity and Bioadhesive Properties of Poly-N-Isopropylacrylamide Hydrogel. *Heliyon* 2019, *5* (4), e01474. https://doi.org/10.1016/j.heliyon.2019.e01474.

(21) Dutta, L.; Mondal, A.; Ramasastry, S. S. V. Metal-Free Reductive Aldol Reactions. *Asian J. Org. Chem.* 2021, *10* (4), 680–691. https://doi.org/10.1002/ajoc.202000693.

(22) Mase, N.; Nakai, Y.; Ohara, N.; Yoda, H.; Takabe, K.; Tanaka, F.; Barbas, C. F. Organocatalytic Direct Asymmetric Aldol Reactions in Water. *J. Am. Chem. Soc.* 2006, *128* (3), 734–735. https://doi.org/10.1021/ja0573312.

(23) List, B.; Hoang, L.; Martin, H. J. New Mechanistic Studies on the Proline-Catalyzed Aldol Reaction. 4.

(24) Emma, M. G.; Tamburrini, A.; Martinelli, A.; Lombardo, M.; Quintavalla, A.; Trombini, C. A Simple and Efficient Protocol for Proline-Catalysed Asymmetric Aldol Reaction. *Catalysts* 2020, *10* (6), 649. https://doi.org/10.3390/catal10060649.

(25) List, B.; Lerner, R. A.; Barbas, C. F. Proline-Catalyzed Direct Asymmetric Aldol Reactions. *J. Am. Chem. Soc.* 2000, *122* (10), 2395–2396. https://doi.org/10.1021/ja994280y.

(26) Adv Synth Catal - 2019 - Vachan - Proline and Its Derivatives as Organocatalysts for Multi- Component Reactions in Aqueous.Pdf.

(27) Hu, Y.; Tian, Z.-Y.; Xiong, W.; Wang, D.; Zhao, R.; Xie, Y.; Song, Y.-Q.; Zhu, J.; Lu, H. Water-Assisted and Protein-Initiated Fast and Controlled Ring-

Opening Polymerization of Proline *N* -Carboxyanhydride. *Natl. Sci. Rev.* 2022, nwac033. https://doi.org/10.1093/nsr/nwac033.

(28) Contreras-Cáceres, R.; Leiva, M. C.; Ortiz, R.; Díaz, A.; Perazzoli, G.; Casado-Rodríguez, M. A.; Melguizo, C.; Baeyens, J. M.; López-Romero, J. M.; Prados, J. Paclitaxel-Loaded Hollow-Poly(4-Vinylpyridine) Nanoparticles Enhance Drug Chemotherapeutic Efficacy in Lung and Breast Cancer Cell Lines. *Nano Res.* 2017, *10* (3), 856–875. https://doi.org/10.1007/s12274-016-1340-2.

(29) Kumar, A.; Dewan, M.; De, A.; Saxena, A.; Aerry, S.; Mozumdar, S. Aldol Condensation in PEG-400 Catalyzed by Recyclable L -Proline Supported on Nano Gold Surface. *RSC Adv* 2013, *3* (2), 603–607. https://doi.org/10.1039/C2RA22522K.

(30) Jaradat, D. M. M. Thirteen Decades of Peptide Synthesis: Key Developments in Solid Phase Peptide Synthesis and Amide Bond Formation Utilized in Peptide Ligation. *Amino Acids* 2018, *50* (1), 39–68. https://doi.org/10.1007/s00726-017-2516-0.

(31) Dai, Y.; Yue, N.; Huang, W.; Qian, H. Fragment Synthesis of Disulfide-Containing Peptides. *MethodsX* 2020, *7*, 100945. https://doi.org/10.1016/j.mex.2020.100945.

(32) Khlebtsov, B. N.; Khlebtsov, N. G. On the Measurement of Gold Nanoparticle Sizes by the Dynamic Light Scattering Method. *Colloid J.* 2011, *73* (1), 118–127. https://doi.org/10.1134/S1061933X11010078.

(33) Dong, J.; Carpinone, P. L.; Pyrgiotakis, G.; Demokritou, P.; Moudgil, B. M. Synthesis of Precision Gold Nanoparticles Using Turkevich Method. *KONA Powder Part. J.* 2020, *37* (0), 224–232. https://doi.org/10.14356/kona.2020011.

(34) Dominguez-Medina, S.; Blankenburg, J.; Olson, J.; Landes, C. F.; Link, S. Adsorption of a Protein Monolayer via Hydrophobic Interactions Prevents Nanoparticle Aggregation under Harsh Environmental Conditions. *ACS Sustain. Chem. Eng.* 2013, *1* (7), 833–842. https://doi.org/10.1021/sc400042h.

(35) BSA.Html.

(36) Mir, M. M.; Majid Fazili, K.; Abul Qasim, M. Chemical Modification of Buried Lysine Residues of Bovine Serum Albumin and Its Influence on

Protein Conformation and Bilirubin Binding. *Biochim. Biophys. Acta BBA - Protein Struct. Mol. Enzymol.* 1992, *1119* (3), 261–267. https://doi.org/10.1016/0167-4838(92)90212-V.

(37) El-Faham, A.; Albericio, F. Carpino's Protecting Groups, beyond the Boc and the Fmoc. *Pept. Sci.* 2020, *112* (4). https://doi.org/10.1002/pep2.24164.

(38) Lu, H.; Wang, J.; Song, Z.; Yin, L.; Zhang, Y.; Tang, H.; Tu, C.; Lin, Y.; Cheng, J. Recent Advances in Amino Acid N-Carboxyanhydrides and Synthetic Polypeptides: Chemistry, Self-Assembly and Biological Applications. *Chem Commun* 2014, *50* (2), 139–155. https://doi.org/10.1039/C3CC46317F.

(39) Sorci, M.; Belfort, G. Insulin Oligomers. In *Bio-nanoimaging*; Elsevier, 2014; pp 233–245. https://doi.org/10.1016/B978-0-12-394431-3.00021-3.

(40) Rohl, C. A.; Baldwin, R. L. Comparison of NH Exchange and Circular Dichroism as Techniques for Measuring the Parameters of the Helix−Coil Transition in Peptides. *Biochemistry* 1997, *36* (28), 8435–8442. https://doi.org/10.1021/bi9706677.

(41) Wischke, C. Fluorescein Isothiocyanate Labelled Bovine Serum Albumin (FITC-BSA) as a Model Protein Drug: Opportunities and Drawbacks. 2006, 5.

(42) Matyjaszewski, K.; Davis, T. P. *Handbook of Radical Polymerization*; John Wiley & Sons, 2003.

(43) Schneider, H. A. Flexibility and Phase Transitions of Polymers. *J. Appl. Polym. Sci.* 2003, *88* (6), 1590–1599. https://doi.org/10.1002/app.11834.

(44) Rodríguez-Fernández, J.; Pérez-Juste, J.; Mulvaney, P.; Liz-Marzán, L. M. Spatially-Directed Oxidation of Gold Nanoparticles by Au(III)−CTAB Complexes. *J. Phys. Chem. B* 2005, *109* (30), 14257–14261. https://doi.org/10.1021/jp052516g.

(45) Lim, Jonghui; Lee, Na-Eun; Lee, Eun-Ji; Yoon, Sangwoon. Surface Modification of Citrate-Capped Gold Nanoparticles Using CTAB Micelles. *Bull. Korean Chem. Soc.* 2014, *35* (8), 2567–2569. https://doi.org/10.5012/BKCS.2014.35.8.2567.

(46) Elliott, A. D. Confocal Microscopy: Principles and Modern Practices. *Curr. Protoc. Cytom.* 2020, *92* (1). https://doi.org/10.1002/cpcy.68.

(47) Li, L.; Xu, L.-W.; Ju, Y.-D.; Lai, G.-Q. Asymmetric Direct Aldol Reactions Catalyzed by a Simple Chiral Primary Diamine–Br⊘nsted Acid Catalyst in/on Water. 13.

(48) Kumar, A.; Dewan, M.; De, A.; Saxena, A.; Aerry, S.; Mozumdar, S. Aldol Condensation in PEG-400 Catalyzed by Recyclable L -Proline Supported on Nano Gold Surface. *RSC Adv* 2013, *3* (2), 603–607. https://doi.org/10.1039/C2RA22522K.

(49) Peme, T.; Brady, D.; Juma, W.; Makatini, M. Development of Fructose-1,6-Bisphosphate Aldolase Enzyme Peptide Mimics as Biocatalysts in Direct Asymmetric Aldol Reactions. *RSC Adv.* 2021, *11* (58), 36670–36681. https://doi.org/10.1039/D1RA06616A.

(50) Runikhina, S.; Eremin, D.; Chusov, D. Reductive Aldol-type Reactions in the Synthesis of Pharmaceuticals. *Chem. – Eur. J.* 2021, *27* (62), 15327–15360. https://doi.org/10.1002/chem.202101768.

(51) Ryan, D. G.; O'Neill, L. A. J. Krebs Cycle Rewired for Macrophage and Dendritic Cell Effector Functions. *FEBS Lett.* 2017, *591* (19), 2992–3006. https://doi.org/10.1002/1873-3468.12744.

ACKNOWLEDGMENTS

Ringrazio il mio relatore, il professore Alessandro Moretto per la pazienza e il costante supporto durante tutto il periodo di tirocinio fino all'ultimo giorno di stesura della tesi, grazie anche per essersi preso il rischio di avere una biotecnologa in un laboratorio chimico; grazie anche a Matteo Pollastrini, per i suggerimenti "chimici" e le spiegazioni.

Ringrazio la mia controrelatrice, la professoressa Silvia Gross che durante gli incontri mi ha saputo dare utili consigli per migliorare alcuni aspetti del progetto.

Ringrazio infine i miei genitori, Alessia ed i miei nonni, le persone che più mi hanno sostenuta dal primo all'ultimo esame e che mi hanno permesso di raggiungere questo obiettivo.